DESIGN AND TESTING OF COLLIMATORS FOR USE IN MEASURING X-RAY ATTENUATION

By

RAJESH PANTHI

Master of Science (M.Sc.) in Physics

Tribhuvan University

Kathmandu, Nepal

2009

Submitted to the Faculty of the
Graduate College of the
Oklahoma State University
in partial fulfillment of
the requirements for
the Degree of
MASTER OF SCIENCE
December, 2017

DESIGN AND TESTING OF COLLIMATORS
FOR USE IN MEASURING X-RAY
ATTENUATION

Thesis Approved:

Dr. Eric R. Benton

Thesis Adviser and Chair

Dr. Eduardo G. Yukihara

Dr. Mario F. Borunda

ACKNOWLEDGEMENTS

I would like to express the deepest appreciation to my thesis adviser Associate Professor Dr. Eric Benton of the Department of Physics at Oklahoma State University for his vigorous guidance and help in the completion of this work. He provided me all the academic resources, an excellent lab environment, financial assistantship, and all the lab equipment and materials that I needed for this project. I am grateful for many skills and knowledge that I gained from his classes and personal discussion with him.

I would like to thank Adjunct Profesor Dr. Art Lucas of the Department of Physics at Oklahoma State University for guiding me with his wonderful experience on the Radiation Physics. My sincere thank goes to the members of my thesis committee: Professor Dr. Eduardo G. Yukihara and Assistant Professor Dr. Mario Borunda of the Department of Physics at Oklahoma State University for generously offering their valuable time and support throughout the preparation and review of this document.

I would like to thank my colleague Mr. Jonathan Monson for helping me to access the Linear Accelerators (Linacs) in St. Francis Heart Hospital at Tulsa, OK for the experimental work of this project. I am grateful for the informative discussions with my lab mate, Oliver Causey.

Finally, I am deeply thankful to my parents, wife and son for their spiritual support and inspiration throughout my life.

Name: RAJESH PANTHI

Date of Degree: DECEMBER, 2017

Title of Study: DESIGN AND TESTING OF COLLIMATORS FOR USE IN MEASURING X-RAY ATTENUATION

Major Field: MEDICAL PHYSICS

Abstract:

The main goal of this project was to design and test a set of collimators for use in measuring x-ray attenuation. Two collimators: a primary collimator and a secondary collimator, were built. The primary collimator was built using 10.0 cm of lead, followed by 7.0 cm of tin, 1.5 mm of copper and 0.5 mm of aluminum, in the respective order. A 1.5 mm thick, copper filter was also used on the aperture of the primary collimator. The secondary collimator was built using 2.5 cm of lead. The cross-sectional size of both the collimators was made to be 15×15 cm^2. The shape of the aperture in each collimator was made to be 1.5 cm $\times$ 3.0 cm. Various features of the collimators were tested in the Varian TrueBeam and Varian Trilogy linear accelerators. The primary collimator was found to best minimize the secondaries produced by the various components inside the gantry and the collimator itself that reach the absorber, when placed at least 30.0 cm away from the absorber upstream the beam. The copper filter in the primary collimator was found unnecessary. The secondary collimator was found to best minimize the secondaries produced by the absorber that reach the detector, when placed atleast 20.0 cm away from the detector upstream the beam. With both the collimators placed at their optimal positions, the cross-sectional size of the collimated beam measured around the detector, placed at 200 cm from the source, was found to be approximately equal to 1.5 cm $\times$ 3.0 cm. The cross-sectional size of the collimated beam at the position of absorber was found to be 1.9 cm $\times$ 4.3 cm and that of attenuated x-ray beam was found to be 3.0×5.5 cm.

TABLE OF CONTENTS

LIST OF TABLES

LIST OF FIGURES

Chapter 1

INTRODUCTION

A beam of x-rays produced by an x-ray machine used in clinics, either by an x-ray tube or a linear accelerator (linac), is always heterogeneous in energy. The photons in clinical x-ray beam can have energy between some minimum value, E_{min}, determined by the amount of filtration that the beam passes through, and a maximum value, E_{max}, determined by the voltage applied to accelerate the electrons towards the electron target. For example, a beam of $120\,kVp$ x-rays will have photons with energies from few keV to $120\,keV$. [3]

An accurate knowledge of the energy spectrum of a clinical x-ray beam is of great importance. In mammography, the knowledge of x-ray spectra can be used to optimize the image quality and to optimize the dose in mammary glands with a variety of anode-filter combinations [4]. In other diagnostic x-ray imaging, the energy spectrum is used for the calculation of the absorbed dose in a patient during a clinical scan. In computed tomography(CT), knowledge of the energy spectrum helps to reduce the beam hardening artifacts, implementing dual-energy methods, and performing qualitative CT [5]. For both the diagnostic and therapeutic x-rays, an energy spectrum of x-rays is used for a calculation of spectrum-averaged dosimetric quantities such as radiation weighted dose, effective dose, radiation weighting factors, etc. and detector correction factors [6]. Additionally, the quality of a beam of x-rays can only be described completely by using an accurate knowledge of the beam's energy

spectrum. It is known that the x-ray source spectrum can drift over time and repeated usage [5]. So, as it is directly related to diagnostic and therapy dose calculation, the determination of x-ray energy spectra needs to be performed on a regular basis.

Despite the great importance of determining x-ray energy spectrum, it is very difficult to determine the spectrum either experimentally or theoretically. Historically, there are three main methods of determining the spectrum of x-rays: 1) direct measurement, 2) theoretical calculation, and 3) deconvolution of attenuation data of the beam measured under a narrow beam geometry.

The direct measurement of x-ray energy spectrum is possible by using scintillation or Silicon detector spectroscopy techniques only when the photon flux is relatively low in order to avoid saturating the detector. Since all the x-ray machines that are used in clinics have a high flux, any detector that we place in the beam quickly becomes saturated with too much signal and is unable to accurately measure the original energy spectrum of the beam.

The theoretical calculation of an x-ray energy spectrum, often using Monte Carlo methods, is very old and powerful method, but requires detailed information about the geometry of the x-ray machine and the material environment through which the beam passes. Due to the propriety nature of x-ray equipment manufacturers, it is often impossible to get the detailed information needed concerning the internal components of the machine itself. Additionally, each machine has a unique geometry so that it is often very time consuming and difficult to use the calculation method that works in one geometry for a different machine with even a slightly different geometry. The theoretical approach can be used to determine x-ray energy spectra, but not on a routine basis.

The method based on attenuation data has been found to be one of the

best in estimating x-ray energy spectra for both diagnostic and therapeutic x-ray machines [7–12] . This method requires attenuation data measured under a narrow beam geometry. Attenuation data is a set of measured intensities, often in terms of exposure in air, of attenuated beam by an absorber of various thicknesses. There are few different methods such as singular value decomposition (SVD), expectation maximization (EM), iterative that determine x-ray energy spectrum using measured attenuation datasets. In a method, an initial guess to the true x-ray energy spectrum is made in the beginning. Then the guess spectrum is improved by an iterative process of minimizing the differences between measured and calculated transmission data sets. The choice of absorber material plays a very important role in the uniqueness of the x-ray spectrum derived from attenuation data. The mass attenuation coefficient of the absorber material must have decreasing values in the photon energy range being determined.

The goal of my research is to develop a computer program that estimates original energy spectrum of high-intensity x-ray beams based on measured attenuation data from the beam. For a better accuracy of the estimated x-ray spectrum, attenuation data should be measured in such a way that the detector measures the attenuation of only the primary photons and not secondary or scattered photons. X-rays produced by the electron target, located inside the gantry, interact with various components in between the source and the absorber, such as flattening filters, the jaws in the gantry, air, etc. producing secondary x-rays before reaching the absorber. Secondary x-rays are also produced in the absorber while the beam passes through it. The contamination due to the secondary photons makes it impossible to measure the attenuation of only the primary photons. In order to measure attenuation of only the primary photons, we need a narrow beam of primary photons with the cross-sectional size just large enough to cover the radiation sensitive region of the detector to ensure all the primary photons that do not undergo any interaction in the absorber are counted in the detector, while

minimizing the number of secondary photons that reach the detector.

The main objectivee of this M.S. thesis project were to design and test a set of collimators for use in measuring attenuation data sets to be used in accurately determining the energy spectra of therapeutic x-ray beams. For this purpose, I:

1. studied the origin of secondary x-rays while measuring an attenuation data,
2. designed and built a pair of collimators: a primary collimator to be used to minimize the secondary x-rays generated in between the source and an absorber, and a secondary collimator to be used to minimize the secondary x-rays generated in between the absorber and detector,
3. determined the optimal position of each collimator for a narrow beam geometry, and
4. measured the radial distribution of the intensity of beam beyond each of the collimators.

Chapter 2

THEORY

2.1 Determining x-ray spectra based on attenuation data

Figure 2.1 shows a parallel beam of x-rays, consisting of N_o photons with n different energies $(E_1, E_2, ..., E_n)$ incident on a layer of material of thickness x. The number of photons that pass through the material without undergoing any interaction, $N(x)$, is given by,

$$N(x) = \sum_{j=1}^{n} N_{oj} e^{-\mu(E_j)x}, \tag{2.1}$$

where N_{oj} is the number of photons with energy E_j before entering the absorber and $\mu(E_j)$ is the total mass absorption coefficient for photons of energy E_j of the particular material through which the beam is passing and is usually expressed in cm^2/gm or m^2/kg. In other words, $\mu(E_j)$ is the fraction of photons with energy E_j that interact per unit thickness of the attenuator. [13]

Experimentally, $N(x)$ is measured by a detector such as an ionization chamber, often in terms of exposure in air. A set of measured values of $N(x)$ for absorbers of varying thicknesses (x) is called attenuation data set. An attenuation data set measured with m different thicknesses of an absorber can be represented by the following

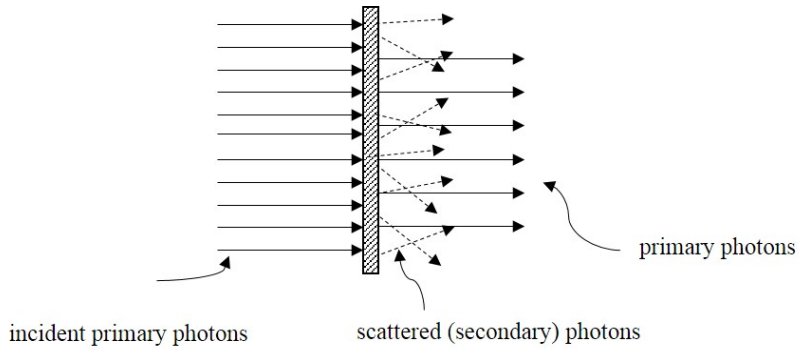

Figure 2.1: Attenuation of a beam of x-rays.

equation:

$$N(x_i) = \sum_{j=1}^{n} N_{oj} e^{-\mu(E_j)x_i}, i = 1, 2, ..., m \tag{2.2}$$

where N_{oj} $(j = 1..n)$ is the number of primary photons with energy E_j before passing through the absorber.

Once we measure an attenuation data set, the quantities $N(x_i)$, x_i, and $\mu(E_j)$ in equation 2.2 are known and N_{oj} is the only unknown quantity. By solving equation 2.2 for N_{oj}, we can determine the energy spectrum of an x-ray beam. Since we can measure $N(x)$ with absorber of certain number of different thicknesses, we have only few (m) equations for many (n) unknowns and hence the solution to equation 2.2 is not unique.

Additionally, equation 2.2 is valid only if all the primary photons that do not undergo any interaction with the absorber are counted in $N(x_i)$ and the rest of the primary photons are either absorbed in or scattered away from the absorber, so that none of the secondary photons produced in the absorber reach the detector. If the detector receives any secondary photons along with the primary photons and includes in $N(x_i)$, then the equation 2.2 no longer remains valid. Since the system of equations 2.2 is already under-determined, any complexity introduced by the contamination of the secondary photons makes the problem even more difficult. Therefore a major

problem associated with the method of determining x-ray spectrum from attenuation data is to minimize or eliminate the secondary photons that reach the detector. The accuracy of the estimated x-ray spectrum also depends on some other factors such as the choice of the absorber material, type of detector used, etc. which will be taken account elsewhere.

2.2 Sources of secondary x-rays in the measurement of attenuation data sets

A therapeutic x-ray beam is produced by a linear accelerator in which the electron target (source) is located inside the gantry and has a very high intensity. The primary x-rays produced from the source travel through various components such as the flattening filter, the collimating jaws and any other additional filters before exiting the gantry. The primary x-rays interact with the material of these various components and produce secondary x-rays.

When a beam of x-rays passes through a material, the x-rays may interact with the material by one of the major three mechanisms: 1) incoherent or Compton scattering, 2) photoelectric effect, and 3) pair production. A less important process called coherent or Rayleigh scattering also takes place, but at only a negligibly small level. The type of interaction that a photon has mainly depends on its energy and the type of material through which it passes. A photon might also go through multiple processes before it is completely absorbed or scattered by the material. Since an x-ray beam is always polyenergetic, photons will undergo all types of interaction while passing through an absorber. [3]

Depending on the type of interaction that an x-ray photon undergoes with

the material, the photon may either be scattered with or without loosing its energy or may generate charged or uncharged secondary particles. When a photon interacts with the material by any process(es), it is no longer considered a primary photon. And photons generated as a result of an interaction are considered secondary photons. The major three types of interaction that produces the secondary x-rays while measuring attenuation data sets are explained below.

2.2.1 Photoelectric effect

Figure 2.2 shows a diagram illustrating the production of characteristic x-rays as a result of the photoelectric effect. In this interaction, a photon of energy hν collides with an atom and transfers all of its energy to one of the bound electrons on the K, L, M, or N shells, so that the electron is ejected out. A part of the incident photon's energy, equal to the binding energy of the shell from which the electron is ejected (E_s), is used to free the electron from its shell. The ejected electron, called a photoelectron, carries away the remaining energy (hν- E_s) in the form of its kinetic energy. The photoelectron travels only a relatively short distance and rapidly loses its energy. Therefore the energy of the incident photon is deposited in the matter close to the site of photoelectric interaction. The vacancy created by the ejected electron is filled up by a transition of one of the outer shell electrons thereby releasing a photon, called characteristic x-ray.

It is also possible that the excess energy during the process of downward transition in an excited or ionized atom is given to one of the outer electrons and this electron is then ejected from the atom. The electron emitted from such process is called Auger electron. The energy of an Auger electron is equal to the energy lost by the incident electron minus the binding energy of the electron that is ejected from the

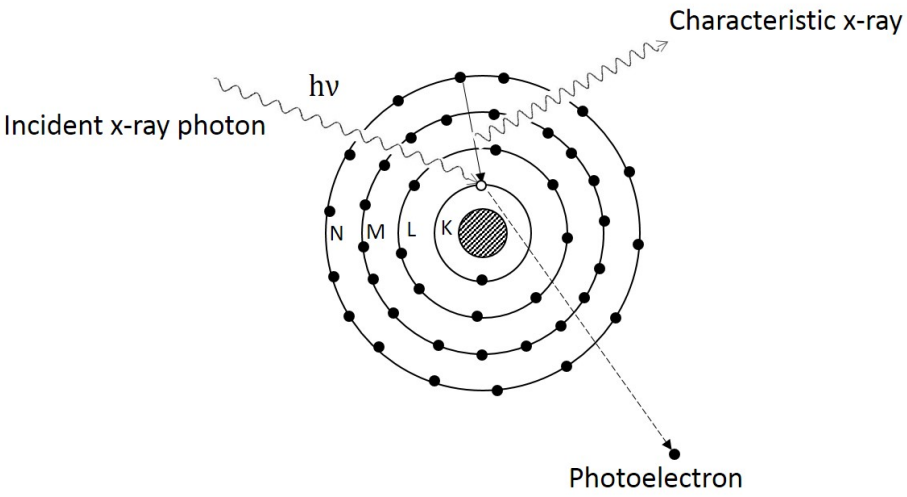

Figure 2.2: Diagram illustrating the emission of characteristic x-rays as a result of the photoelectric process.

atom. The relative probability of the emission of characteristic x-ray to the emission of an Auger electron, called the fluorescent yield, increases with the increase of the atomic number of the target elements. [3]

The cross-section of the photoelectric process depends on the energy of the incident photon and the atomic number of the material. Figure 2.3 shows a plot of the mass photoelectric coefficient as a function of photon energy for tungsten (Z = 74), representing high Z material, and aluminum (Z = 13), representing low Z material. The photoelectric process is most likely to occur if the energy of the incident photon is just greater than the binding energy of the electron. Energies just less than binding energy cannot eject the electron and therefore the cross section varies with energy in a complicated way with discontinuities at the energy corresponding to each shell or sub-shell. For low energy photons ($\lesssim$ 1 MeV), the photoelectric cross section between the peaks varies with the photon energy approximately as $1/(h\nu)^3$. The photoelectric cross section per atom depends upon approximately Z^4 for high Z materials and on $Z^{4.8}$ for low Z materials.

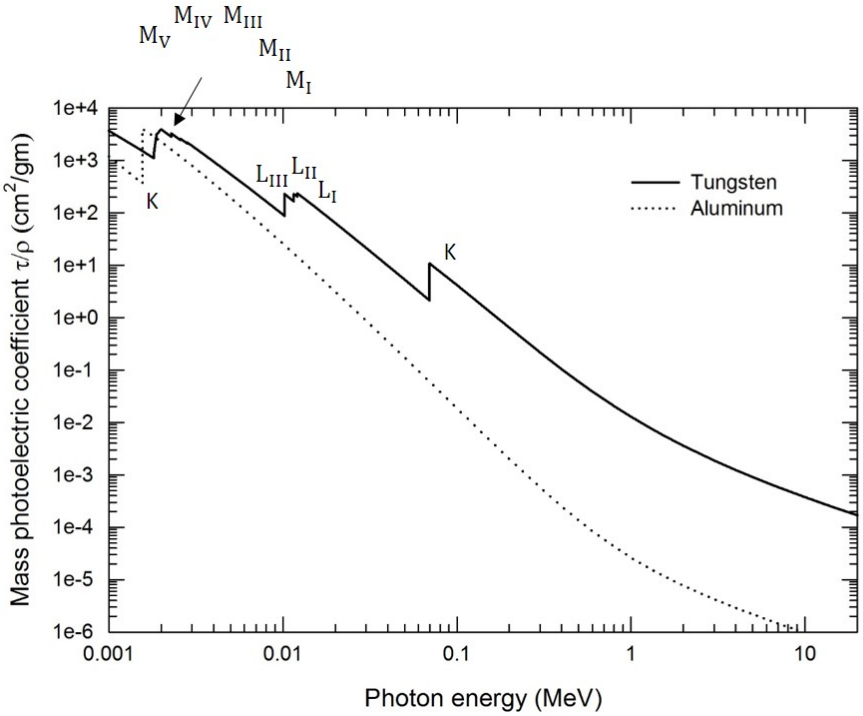

Figure 2.3: Mass absorption coefficients corresponding to the photoelectric process as a function of photon's energy.

2.2.2 Incoherent or Compton scattering

Compton scattering is a very common type of interaction that x-rays have with the medium through which they pass. In this process, an x-ray photon collides with a nearly free electron and transfers some of its energy to the electron and the electron travels away at some angle θ off the direction of incident photon, as shown in Figure 2.4. The incident photon with reduced energy scatteres off in a different direction, at a different angle ϕ. The amount of energy transferred to the electron in a Compton scattering depends on the energy of the photon and the angle at which the photon scatters relative to its incoming direction [3].

The cross section of the Compton scattering depends mainly on the energy of incident photon and is almost independent of atomic number of the medium because it essentially involves only free electrons [14]. The mass absorption cross-section cor-

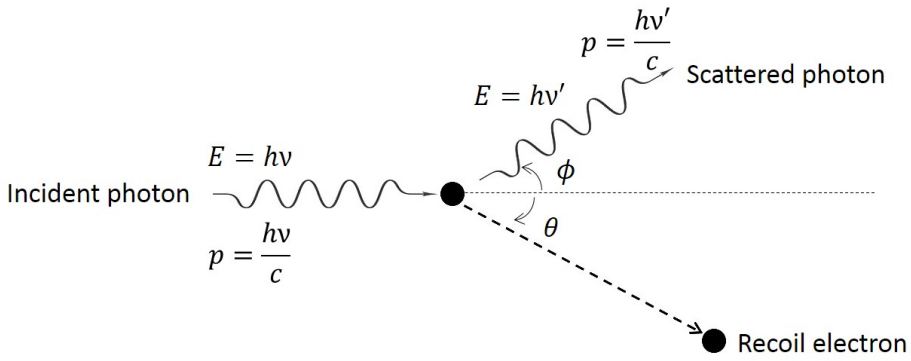

Figure 2.4: Diagram illustrating the Compton scattering of an x-ray photon by a free electron.

responding to the Compton scattering as a function of photon energy in two different elements: tungsten and aluminum, are shown in Figure 2.5 [1].

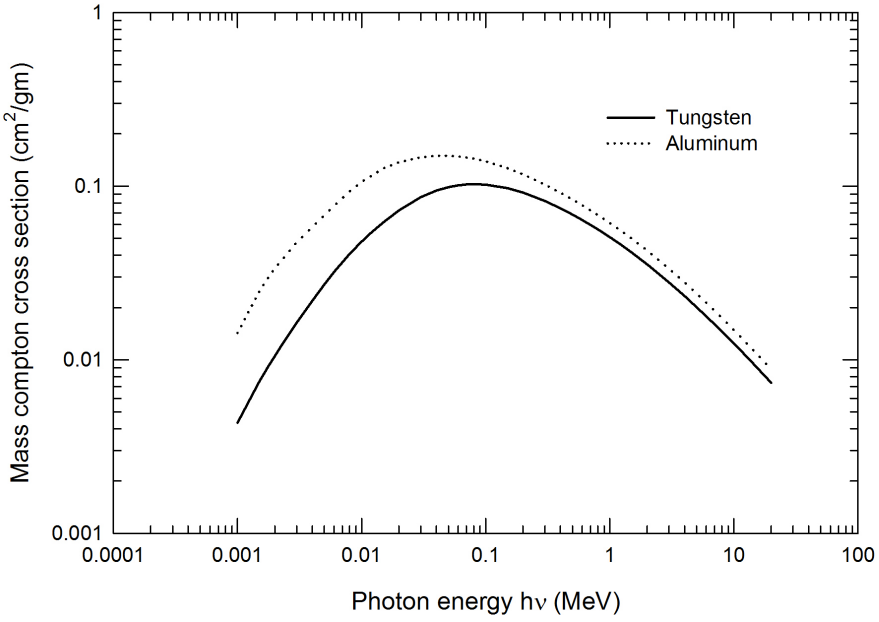

Figure 2.5: Mass absorption coefficients corresponding to the Compton scattering process as a function of photon energy.

The mathematical expression for the cross section of the Compton scattering was derived by J.J. Thomson using the classical theory of electromagnetic radiation. The Thomson's scattering cross section formula improved by using quantum theory of

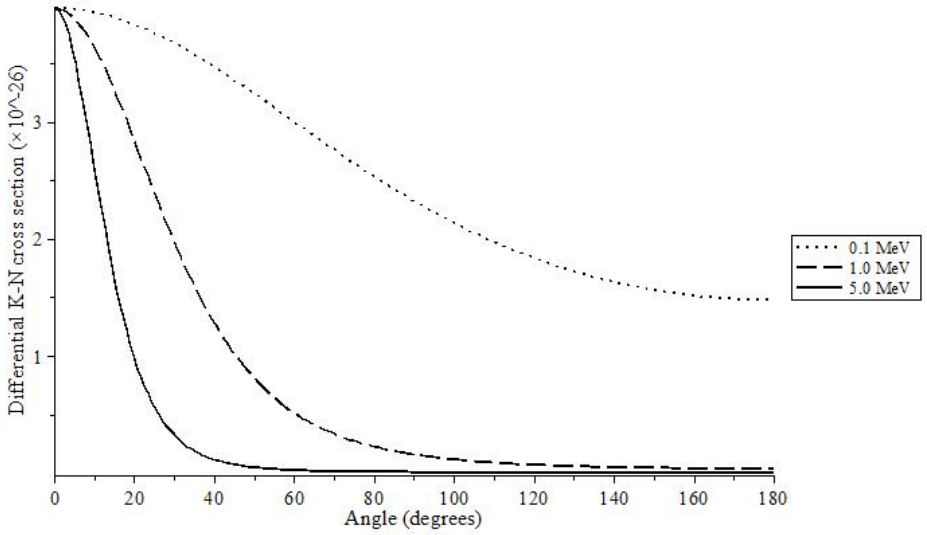

Figure 2.6: The Klein-Nishina's differential cross-section per unit solid angle as a function of the angle of photon scattering for three different energies, $0.1\,MeV, 1.0\,MeV$ and $5.0\,MeV$.

electromagnetic radiation is given by Klein-Nishina formula: [13],

$$\frac{d\sigma_o}{d\Omega} = \frac{r_o^2}{2}(1+\cos^2\theta)\left\{\frac{1}{1+\alpha(1-\cos\theta)}\right\}^2\left\{1+\frac{\alpha^2(1-\cos\theta)^2}{\Big(1+\alpha(1-\cos\theta)\Big)(1+\cos^2\theta)}\right\},$$

where $r_o^2 = 2.81794 \times 10^{-15}\,m$ is the classical electron radius, α is the ratio of the energy of the photon to the rest mass energy of the electron.

A plot of the K-N differential cross-section for three different photon's energy is shown in Figure 2.6 which shows that the majority of the photons get scattered in forward direction, i.e. towards the original direction of the incident photon [3].

Additionally, the kinematics of the Compton scattering, the energy of scattered photon ($h\nu'$) at an angle θ relative to the initial direction of incident photon is given by

$$h\nu' = \frac{h\nu}{1+\left(\frac{h\nu}{m_o c^2}\right)(1-\cos\theta)},$$

where $h\nu$ is the energy of the incident photon. This shows that the photons that are scattered off at small angles loose only small fraction of their initial energy and those scattered off at greater angles loose more energy.

2.2.3 Pair production

When a photon with energy greater than $1.02\,MeV$ interacts strongly with the electromagnetic field of an atomic nucleus then an electron-positron pair is produced and the photon completely disappears. This process is called the pair production. Since the minimum energy that either an electron or positron possess is its rest mass energy, $0.511\,MeV$, the minimum energy that a photon to have pair production is $2 \times 0.511\,MeV$. This is why $1.02\,MeV$ is considered as a threshold energy for a photon to have pair production. If a photon has more than $1.02\,MeV$ the excess energy after having pair production is shared by the electron and the positron as their kinetic energy [14].

The cross section of photons with energy greater than $1.02\,MeV$ to have pair production increases with the increase of the atomic number of the medium Àlthough for diagnostic (kilovolt) x-rays we observe no pair production, we will consider this effect in the calculations involved in megavolt x-rays in this project.

2.3 Total absorption cross section (μ)

The fraction of x-ray photons that interact per unit thickness of an absorber through which they pass is called the total absorption cross section (μ). In other words, μ is the probability that an x-ray photon interacts with a material. Since the relative probability of each type of interaction is proportional to the cross-section for that process, the probability of an interaction (μ) is the sum of the cross-sections: [3]

$$\mu = \tau + \sigma_{coh} + \sigma_{inc} + \kappa, \tag{2.3}$$

where τ is the photoelectric absorption coefficient, σ_{coh} is the coherent (Rayleigh) scattering coefficient, σ_{inc} is the incoherent (Compton) scattering coefficient and κ is the pair production coefficient (sum of the pair production coefficients in the electronic and the nuclear field). In low Z materials, σ_{coh} is usually negligible except at very low energies (< 10 keV).

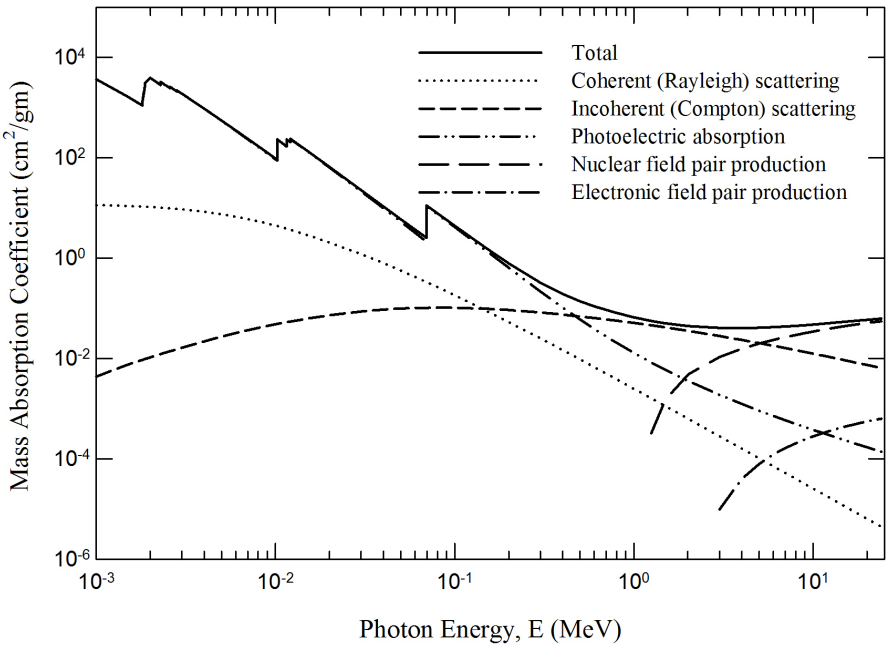

Figure 2.7: Mass attenuation coefficient for various interaction between photons and tungsten. Data is taken from NIST database [1]

Figure 2.7 shows plots of the total mass absorption coefficient and the mass absorption coefficient corresponding to four different interactions on tungsten (Z = 74) as a function of photon energy.

At low energies (< 0.1 MeV), the photoelectric effect dominates all other types of interaction and solely contributes to the total attenuation coefficient. For the photons with energies from 0.1 MeV to 0.5 MeV the interaction is dominated by photoelectric absorption but in this region the photons also have Compton scattering. Both the photoelectric absorption and Compton scattering contribute to the total at-

tenuation coefficient. The Compton scattering dominates all other types of interaction when the photons have energies between 0.5 MeV and 5.0 MeV. Above 5 MeV the pair production dominates all other interactions. And for the x-rays with energies from 1 keV to 25 MeV the mass coherent (Rayleigh) scattering coefficient is very small and contributes negligibly to the total attenuation coefficient.

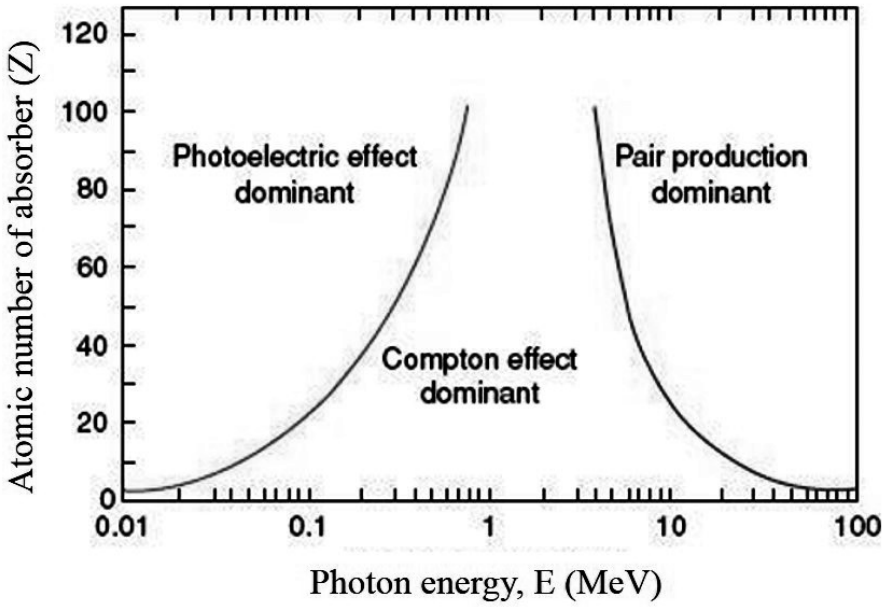

Figure 2.8: Relative importance of three major interactions between the photons and absorbers as a function of photon energy and atomic number of the absorber. [2]

Additionally, Figure 2.8 shows a relative importance of the three major interaction between the photons and the absorbers of different Z. We can see that in the diagnostic radiography, the photoelectric absorption and the Compton scattering are very important (i.e. $\mu = \tau + \sigma_{inc}$). And in the radiation therapy with the unfiltered beams of x-rays, all three interactions should be considered (i.e. $\mu = \tau + \sigma_{inc} + \kappa$). [2]

National Institute of Standards and Technology (NIST) provides a web program called XCOM which can generate the attenuation coefficients for all the elements, compounds and mixtures, at energies between 1 keV and 100 GeV. XCOM

provides total attenuation coefficients and partial cross sections for the following processes: incoherent scattering, coherent scattering, photoelectric absorption, and pair production. The attenuation coefficients obtained from the XCOM program of NIST database are scientifically accepted benchmarks. [15]

2.4 Experimental setup for a narrow beam attenuation

An experimental setup to measure an attenuation data of an x-ray beam on a given material that helps to detect only the primary photons by minimizing any secondary photons and other charged or uncharged particles away from the detector is called a narrow beam geometry or a good geometry [16]. The essential features, that a narrow beam geometry must have, are: [13]

(i) The detector is to be placed far enough from the absorber so that secondary x-rays, even with small angle, will miss the detector, and

(ii) The beam is to be collimated to just cover the radiation sensitive region of the detector so that all the primary x-rays that do not undergo any interaction in the absorber can be counted correctly.

Figure 2.9 shows a diagram of a narrow beam geometry designed for the measurement of attenuation data sets in therapeutic x-ray beams. It consists of two collimators: a primary collimator and a secondary collimator. The primary collimator, placed in between the source and absorber, collimates the beam to a desired cross-sectional size that penetrates the absorber. Additionally, it minimizes the secondary x-rays produced by various components such as flattening filters, the jaws in the gantry,

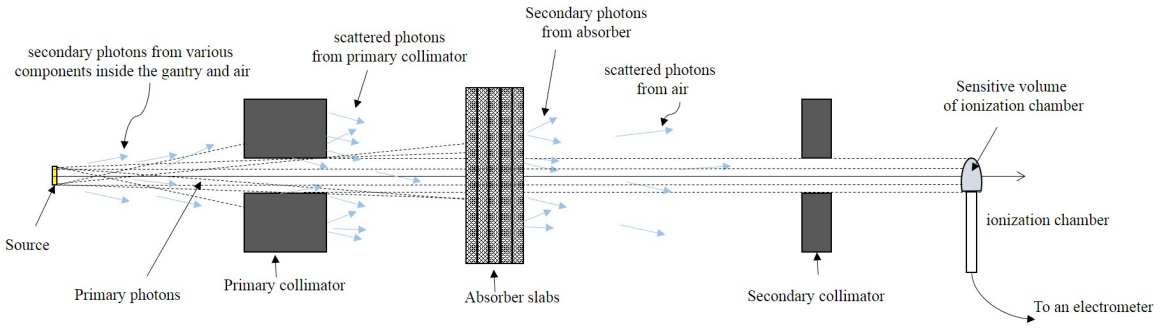

Figure 2.9: Diagram of an experimental setup for the measurement of an attenuation data in a narrow beam geometry.

additional filter, if any, and air present in between the source and absorber. The secondary collimator, placed in between the absorber and the detector, minimizes the secondaries produced by the absorber that reach the detector and allows the primary photons in the attenuated beam to reach the detector.

Chapter 3

METHODOLOGY

3.1 Design of the primary collimator

The role of the primary collimator in an experimental setup for measuring attenuation data in an x-ray beam is:

(i) to reduce the intensity of the scattered (secondary) x-rays from the medium present in between the source and the absorber,

(ii) to reduce the field size of the beam into the desired size,

(iii) to minimize or eliminate intensity of the beam outside the region circumscribed by the collimator, and

(iv) to minimize the characteristic x-rays produced by the inner surface of the collimator's aperture.

A primary collimator with these characteristics was designed and built using four different materials: lead, tin, copper and aluminum.

3.1.1 Material

For the purpose of shielding or collimating x-ray beams, usually a combination of few different materials is used. The use of multiple materials helps to minimize or absorb the secondary x-rays that are produced due to the interaction between the primary x-rays and the material of collimator. For this reason, a combination of four different materials: lead, tin, copper, and aluminum in their respective order was used to build a primary collimator.

3.1.1.1 Lead

Lead (Pb) was used as the main material out of which the primary collimator is made. Lead is one of the cheapest high Z materials and is commonly used in shielding or collimating different ionizing radiations. Compared to other solid materials such as copper, iron, and copper, lead has larger attenuation coefficients (photon absorption cross-sections) for x-rays. The larger mass attenuation coefficient of lead means that there is a greater chance for incident x-rays to interact with lead atoms than with lower Z materials.

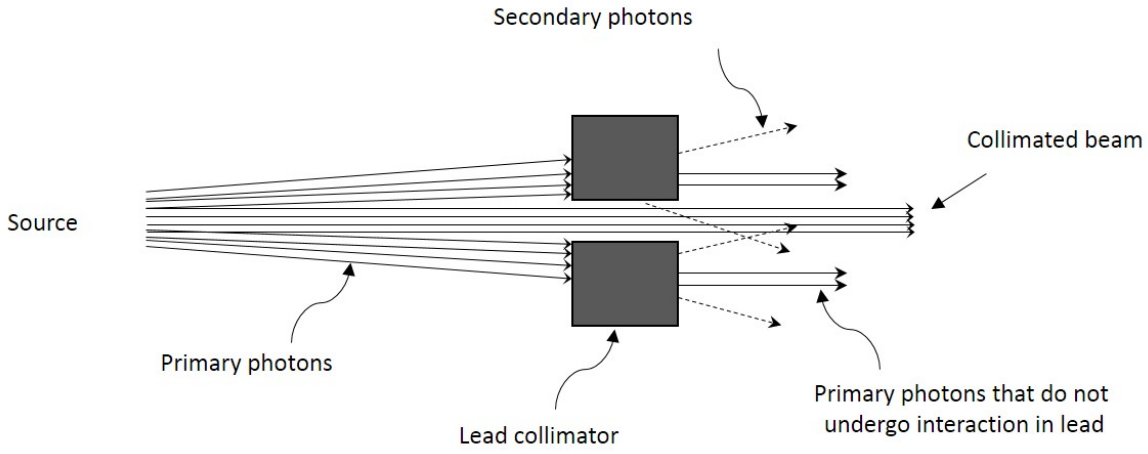

Figure 3.1: A diverging beam of x-rays being collimated by a lead collimator.

Since x-rays do not have finite range in any material, either primary or secondary x-rays are expected from the solid periphery of the collimator's aperture, which can contaminate the collimated beam, as shown in Figure 3.1. In the periphery of the collimated beam, the x-rays can be (i) some of the primary photons that do not undergo any interaction while passing through the solid periphery of the collimator's aperture, (ii) characteristic x-rays corresponding to the absorption lines of Lead, i.e. the photons as a result of photoelectric effect, and (iii) 511 keV photons as a result of annihilation after the pair-production process within the Lead.

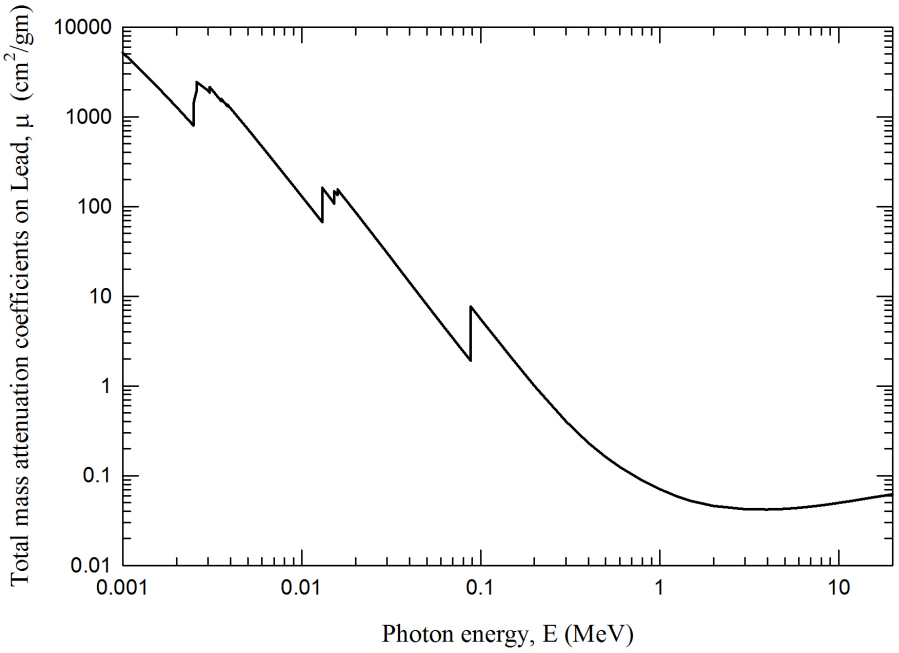

Figure 3.2: Total mass attenuation coefficient for photons in lead as a function of photon energy. [1]

The amount of lead was chosen in such a way that the intensity of the photons of type (i) around the periphery of collimated beam was reduced to less than 1%. The thickness of material required to reduce the intensity of x-rays to $1/100th$ of their initial intensity is called 100^{th} value layer ($x_{1/100}$):

$$x_{1/100} = \frac{\ln\left(\frac{I_o}{I}\right)}{\mu(\mathrm{cm}^{-1})} = \frac{\ln 100}{\mu(\mathrm{cm}^{-1})}. \tag{3.1}$$

Since the photons in an x-ray beam have different energies and hence different values for absorption coefficients (i.e. mass attenuation coefficients, μ), the 100^{th} value layer of lead was calculated by considering the photons that are least likely absorbed in the medium. The photons in the energy range from 1 keV to 20 MeV that are least absorbed in lead have minimum mass attenuation coefficient. Figure 3.2 shows a plot of total mass attenuation coefficients of x-rays (μ) as a function of energy in Lead [1]. The minimum value of μ in Figure 3.2 is $4.197\times\ 10^{-2}$ cm^2/gm or 0.4757 cm^{-1}. Then the required thickness of Lead is:

$$x_{\frac{1}{100}} = \frac{\ln\left(\frac{I_o}{I}\right)}{\mu(\mathrm{cm}^{-1})} = \frac{\ln\left(\frac{100}{1}\right)}{0.4757\,\mathrm{cm}^{-1}} = 9.68\,\mathrm{cm} \approx 10\,\mathrm{cm} \tag{3.2}$$

$10\,cm$ thick lead was chosen to build the primary collimator. To absorb the characteristic x-rays from lead and $511\,keV$ photons as a result of pair production in lead, a layer of tin was used next to lead.

3.1.1.2 Tin

The Lead layer was followed by a layer of tin to absorb the characteristic x-rays produced in the Lead, as well as absorbing 511 keV anhilation photons created as the result of pair production.

The thickness of tin required was decided using the mass attenuation coefficients on tin for the 511 keV photons and the characteristic x-rays from lead, as shown in Table 3.1. The minimum value of the mass attenuation coefficient for photons listed in Table 3.1 is for 511 keV photon and the value is 0.09 cm^2/gm or 0.67 cm^{-1}. The thickness of tin to be placed next to lead was chosen to be 100^{th} value layer for 511 keV photons on tin, i.e. $x_{1/100} = \frac{\ln 100}{0.67\,\mathrm{cm}^{-1}} = 6.84\,\mathrm{cm} \approx 7\,\mathrm{cm}$. This amount of tin in principle reduces the intensity of characteristic x-rays from lead significantly because

Table 3.1: Total mass attenuation coefficients for the photons with energies corresponding to the absorption lines of Lead on Tin. [1]

Absorption Lines of Lead	Energy (keV)	Total absorption coefficient on Tin $\mu(\mathrm{cm}^2/\mathrm{gm})$
M_5	2.48	980.20
$M^{'}4$	2.59	880.90
M_3	3.07	579.30
M_2	3.55	401.80
M_1	3.85	327.70
L_3	13.04	67.81
L_2	15.20	45.00
L_1	15.86	40.10
K	88.00	2.35

of their higher absorption coefficients on tin.

3.1.1.3 Copper

Inclusion of the 7 cm tin layer will lead to the production of some tin characteristic x-rays. To absorb the characteristic x-rays of tin, a layer of copper was used. The required thickness of the copper layer was calculated considering the energy of major characteristic x-rays from tin as listed in 3.2.

Table 3.2: Mass attenuation coefficients for the characteristic photons from Tin on Copper. [1]

Absorption Lines of Tin	Energy (keV)	Total absorption coefficient on Copper $\mu(\mathrm{cm}^2/\mathrm{gm})$
L_3	3.93	364.40
L_2	4.16	313.10
L_1	4.46	257.90
K	29.20	11.77

We can see from Table 3.2 that the K-line from tin, has the minimum value of μ on copper, which is 11.77 $\mathrm{cm}^2/\mathrm{gm}$ or 105.46 cm^{-1}. This value was used to calculate the 100^{th} value layer on copper: $x_{1/100} = \frac{\ln 100}{105.46\,\mathrm{cm}^{-1}} = 0.043\,\mathrm{cm} \approx 0.5\,\mathrm{mm}$.

For practical reasons, 1.5 mm layer of copper was added behind the tin to absorb the tin characteristic x-rays.

3.1.1.4 Aluminum

Finally, to absorb characteristic x-rays produced in copper layer, a layer of aluminum was added behind copper. The thickness of aluminum required was determined considering the energy of the characteristic x-rays from copper and their absorption coefficients on aluminum as shown in Table 3.3.

Table 3.3: Mass attenuation coefficients for the characteristic photons from copper on aluminum. [1]

Absorption Lines of Copper	Energy (keV)	Total absorption coefficient on Aluminum $\mu(\text{cm}^2/\text{gm})$
L_1	1.10	927.90
K	8.98	35.94

Using the minimum value of μ, which is 35.94 cm^2/gm or 97.04 cm^{-1} for K-line of Copper, the 100^{th} value layer on Aluminum was calculated: $x_{1/100} = \frac{\ln 100}{96.998\,\text{cm}^{-1}} = 0.047\,\text{cm} \approx 0.5\,\text{mm}$. In the collimator a $0.5\,mm$ thick aluminum sheet was added behind Copper.

3.1.1.5 Filtering the characteristic x-rays produced in the aperture

In order to absorb most of the characteristic x-rays produced in the aperture of the primary collimator that travel in the forward direction and contaminate the collimated beam of the primary x-rays, a 0.1108 gm/cm^2 thick copper sheet was used at the back end of the primary collimator's aperture as shown in Figure 3.3.

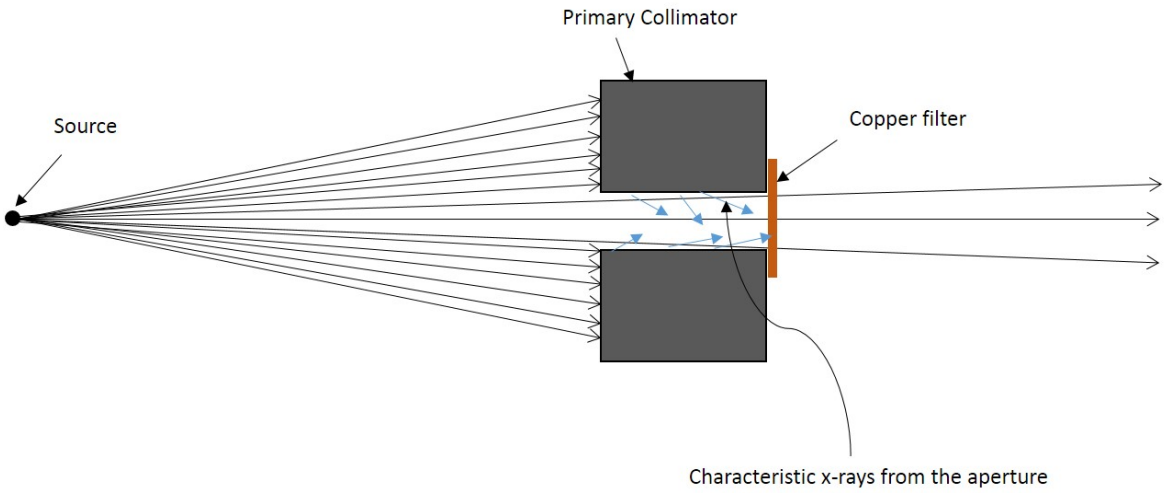

Figure 3.3: Diagram showing a copper filter used to absorb the characteristic x-rays produced in the inner surface of the primary collimator's aperture.

Table 3.4: Calculation of the factors by which different characteristic photons from four different materials of the primary collimator are reduced by a 0.1108 gm/cm^2 thick Copper sheet.

Element	Absorption Lines	Energy (keV)	μ (cm^2/gm)	$\frac{I}{I_o}(=e^{-\mu x})$
Lead	M_5	2.48×10^{-3}	1.23×10^{3}	7.63×10^{-60}
	M_4	2.59×10^{-3}	1.10×10^{3}	1.53×10^{-53}
	M_3	3.07×10^{-3}	7.04×10^{2}	1.35×10^{-34}
	M_2	3.55×10^{-3}	4.78×10^{2}	1.06×10^{-23}
	M_1	3.85×10^{-3}	3.85×10^{2}	3.16×10^{-19}
	L_3	1.30×10^{-2}	1.09×10^{2}	5.47×10^{-6}
	L_2	1.52×10^{-2}	7.14×10^{1}	3.67×10^{-4}
	L_1	1.59×10^{-2}	6.32×10^{1}	9.14×10^{-4}
	K	8.80×10^{-2}	6.09×10^{-1}	9.35×10^{-1}
Tin	L_3	3.93×10^{-3}	3.64×10^{2}	3.06×10^{-18}
	L_2	4.16×10^{-3}	3.12×10^{2}	9.50×10^{-16}
	L_1	4.46×10^{-3}	2.59×10^{2}	3.60×10^{-13}
	K	2.92×10^{-2}	1.18×10^{1}	2.72×10^{-1}
Copper	L_1	1.10×10^{-3}	9.27×10^{3}	0
	K	8.98×10^{-3}	2.78×10^{2}	4.10×10^{-14}
Aluminum	K	1.56×10^{-3}	4.01×10^{3}	2.01×10^{-193}

The thickness of the copper filter was determined by considering the energy

of the major characteristic x-rays from each material used in the primary collimator. The calculation in Table 3.4 shows how the initial intensity of each type of characteristic x-rays (I_o) is reduced while passing through a 0.1108 gm/cm^2 copper sheet. The energies of the absorption lines and attenuation coefficients of these photons on Copper were taken from XCOM NIST database [15]. Very small values of I/I_o for all other characteristic x-rays indicate that these are absorbed completely by Copper filter used.

3.1.2 Dimensions of the primary collimator

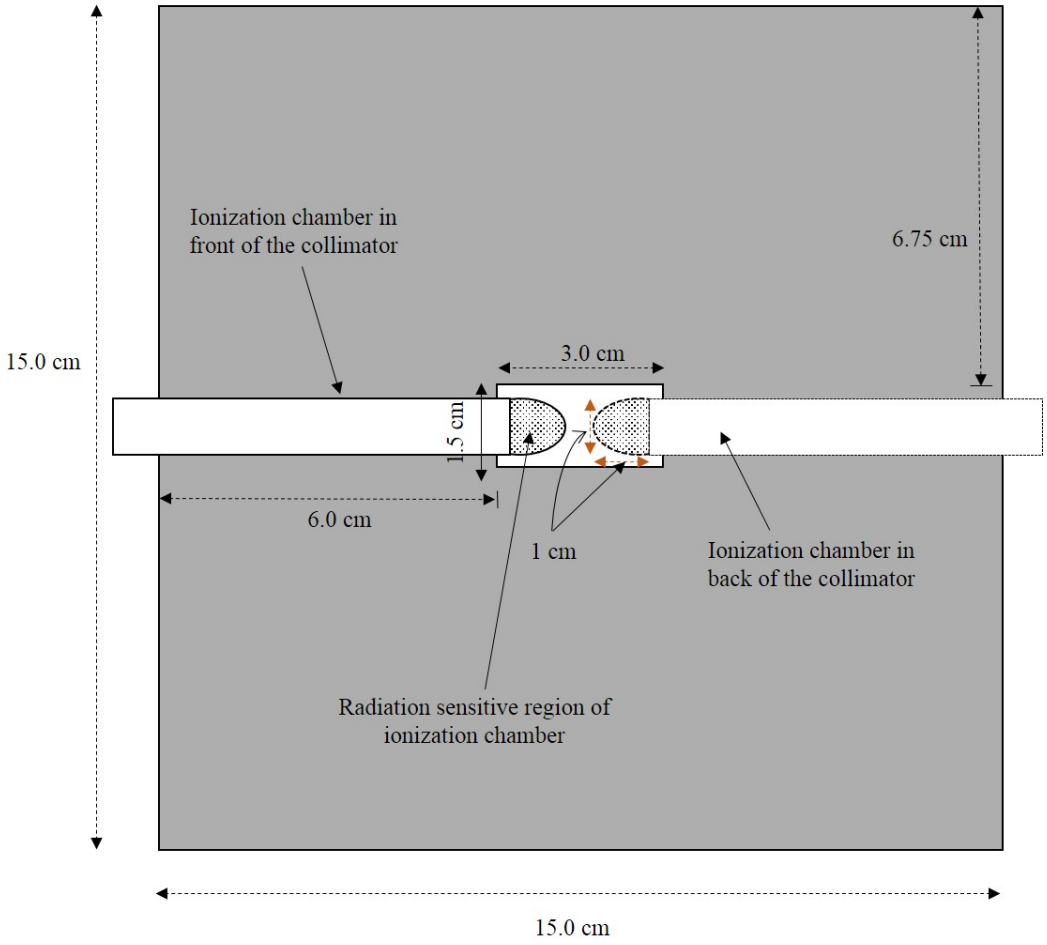

Figure 3.4: Diagram illustrating the dimensions of the collimator aperture.

The aperture shape of the collimator was chosen to be 1.5 cm × 3.0 cm so

that two pin point ionization chambers, each with type number (TN) 31014, manufactured by PTW-Freiburg, could be fitted side by side within the field of the collimated beam. PTW ionization chamber of type 31014 is a vented cylindrical ionization chamber with a radiation sensitive region having a diameter of 2 mm (or 2.9 mm with buildup cap), length of 5 mm, the volume of 0.015 cc, and a reference point on the chamber axis at 3.4 mm from the chamber tip. With the buildup cap, the length of the sensitive volume of the ionization chamber is about 1 cm and the diameter is about 1 cm. Therefore the aperture was chosen to be 1.5 cm $\times$ 1.5 cm for each ionization chamber. Figure 3.4 shows the dimension of the collimator aperture, together with the positioning of the two PTW pinpoint ionization chambers used in measuring attenuation data.

The cross-sectional size of the collimator was made to be 15 $\times$ 15 cm^2 based on size of lead slabs available in the lab. Using the thickness of each material calculated above, the total thickness of the primary collimator is 17.1 cm.

3.1.3 Primary collimator in its assembled form

The collimator was fabricated by the Oklahoma State University (OSU) Physics and Chemistry Instrument Shop. Figure 3.5 shows the primary collimator in its fully assembled form. The collimator consists of 4 slabs of Lead each with the thickness of 2.5 cm, 44 sheets of tin each with the thickness of 0.16 cm, a 1.5 mm thick copper layer and a 1.5 mm thick aluminum sheet stacked in that order. In the case of copper and aluminum, the actual thickness is about 3 times greater than their 100^{th} value layer because these were the thinnest layers of each material available. The total thickness of the collimator was calculated to be 17.34 cm, but the actual thickness measured in the assembled form was about 18.4 cm. The additional thickness was due

to air gaps between the various layers.

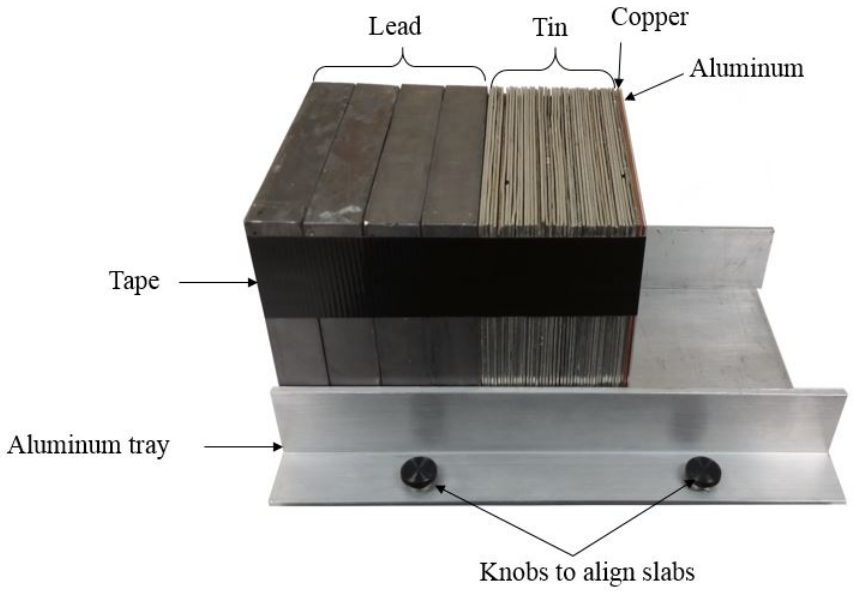

Figure 3.5: Primary collimator in its assembled form.

Front and back views of the primary collimator are shown in Figure 3.6. To improve alignment of the layers on the Aluminum tray the layers were first stacked in proper order, two knobs on the Aluminum tray were tightened and all the layers were taped together as shown in Figures 3.5 and 3.6.

3.2 Design of the secondary collimator

As seen from Figure 2.9 that the role of the secondary collimator is to minimize the number of secondaries, produced in the absorber and in air, that reach the ionization chamber. Some of the features required in the secondary collimator are, (i) it must align perfectly to the primary collimator, (ii) it must be thick enough to reduce the secondaries produced in the primary collimator, the absorber, and in the

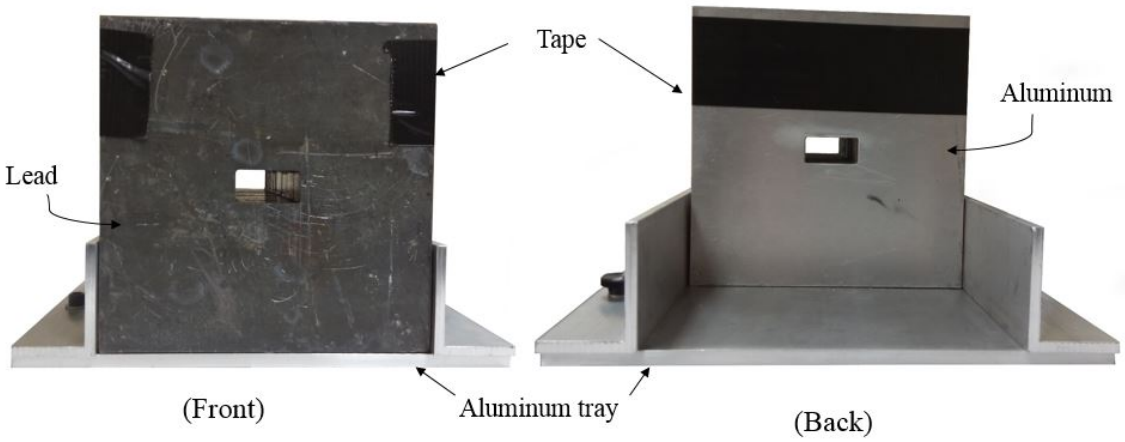

Figure 3.6: The front and the back views of the primary collimator.

air, and (ii) the shape and size of the aperture must be identical to that of the primary collimator so that the primary photons that pass through the primary collimator are not blocked by the secondary collimator.

As mentioned in section 3.1, the solid periphery of the primary collimator reduces the intensity of primary photons around the collimated beam significantly. The x-rays around the collimated beam are further attenuated while passing through absorber. With this assumption, the secondary collimator was made by using only one material: lead. And the thickness of lead was chosen to be 2.5 cm. The aperture of the secondary collimator was also made to be rectangular in shape with the dimensions 1.5 cm $\times$ 3.0 cm.

3.2.1 Secondary collimator in its assembled form

The secondary collimator was also fabricated by the Oklahoma State University (OSU) Physics and Chemistry Instrument Shop. It consists of a single slab of lead with thickness 2.5 cm and the cross-sectional size of 15 cm × 15 cm. For improved alignment, the secondary collimator was mounted on Aluminum tray similar to that used for the primary collimator. Figure 3.7 shows the secondary collimator and its components in assembled form.

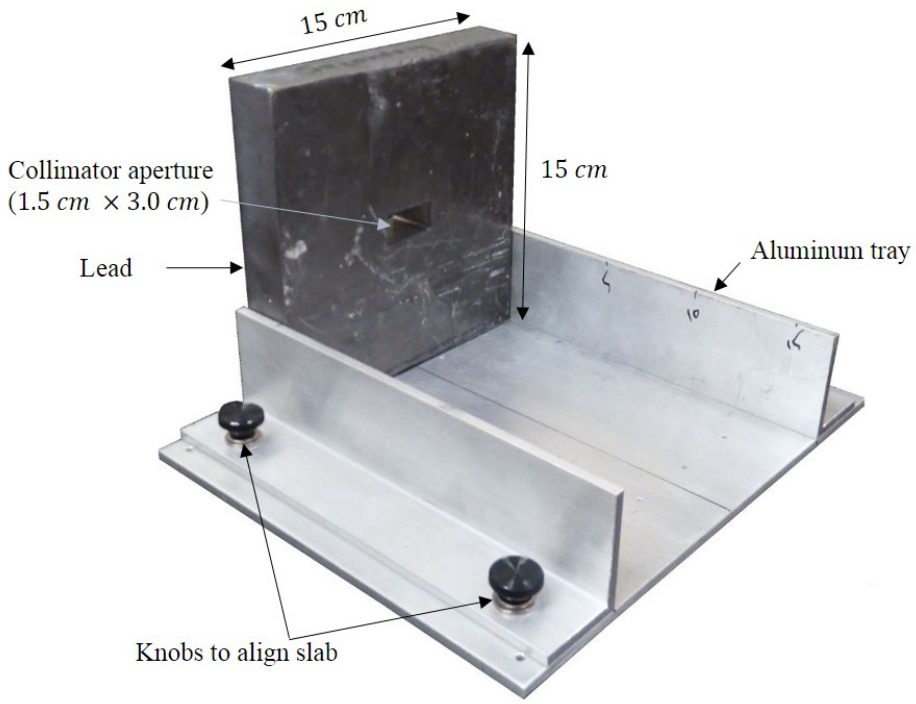

Figure 3.7: Secondary collimator in its assembled form

3.3 Characterization of the primary and secondary collimators

Six different experiments were performed to study various features of the primary and the secondary collimators. The linear accelerators used in these experiments were made available for these experiments by Saint Francis Heart Hospital, Tulsa, OK.

3.3.1 Determination of the optimal position of the primary collimator

(A) Purpose:

The purpose of this experiment was to determine an optimal position for the primary collimator which can sufficiently collimate an x-ray beam at a given distance from the source.

(B) Equipment:

(1) Linear accelerator (Source):

The TrueBeam linear accelerator (model number: 1200), manufactured by Varian, Varian Medical Systems Inc, was used as the source of x-ray beams in this experiment. The Varian Truebeam used in this work is capable of producing x-ray beams with three different nominal energies (6, 10, and 18 MVp) and electron beams with five different energies (6, 9, 12, 16, and 20 MeV). The collimator was mounted on a PerfectPitch^{TM} six degrees of freedom couch for patient positioning

during radiotherapy and radiosurgery procedures.

Only x-ray beams with two different nominal energies, 6 and 10 MVp, were used in this experiment. Various beam properties for each irradiation, such as type of beam, nominal energy of the beam, field size, and the dose was defined from a computer in the control room.

(2) Detector:

PTW pinpoint ionization chamber of type number (TN) 31014 and serial number (SN) 000959, manufactured by PTW-Freiburg (Freiburg, Germany), was used as a detector. It is a commercial ionization chamber that is specially used in absolute dosimetry on x-ray beams with nominal energies between Co-60 and 50 MVp with high spatial resolution. This ionization chamber is suitable for the measurement of dose in small-sized x-ray beams and in relative dosimetry such as output factors, depth dose curves, and beam profiles.

Figure 3.8 shows a diagram of PTW TN31014 ionization chamber. It is a vented cylindrical ionization chamber with a radiation sensitive region having a radius of 1 mm, length of 5 mm, the volume of 0.015 cc, and a reference point on the chamber axis at 3.4 mm from the chamber tip. The wall material of the ionization chamber is graphite with a protective acrylic (Polymethyl methacrylate or PMMA) buildup cap. The wall thickness of the buildup cap is 3 mm. The reference conditions at which this ionization chamber has 100% ion collection efficiency are (i) beam quality Co-60, (ii) temperature of 22^{o}C, (iii) a pressure of 1013.2 hPa, (iv) biasing voltage of +/- 400 V, and (v) a relative humidity of 50%. While taking the measurements, the buildup cap was used.

Figure 3.8: PTW TN31014 ionization chamber.

(3) Electrometer:

The Model 35040 Advanced Therapy Dosimeter (ATD) with serial number 1568043, manufactured by FLUKE Biomedical, USA, was used to read the amount of charge collected in the sensitive area of the ionization chamber. This electrometer is specially used in calibration dosimetry, quality assurance and diagnostic testing of linear accelerators. It features a single channel input with a Triax BNC front/rear connector. It has a measurement accuracy of ± 0.20% reading plus two counts charge and ± 0.20% reading plus two counts current at temperature from 18°C to 28°C. It can supply a biasing voltage between -500 V to +500 V in 0.1 V increments to an ionization chamber. Additionally, it also features timed and continuous charge measurements. Figure 3.9 shows a diagram of FLUKE 35040 electrometer.

A triaxial cable was used to connect the ionization chamber to the FLUKE 35040 electrometer. A biasing voltage of +300 V required for the ionization chamber

Figure 3.9: FLUKE 35040 Advanced Therapy Dosimeter

was supplied from the electrometer. The electrometer was put in the continuous charge measurement mode while taking measurements.

(C) Experimental setup:

Figure 3.10 shows the setup that was used for this experiment. The gantry was set at 90º relative to a vertical axis which provided horizontal x-ray beams from the machine. The primary collimator was placed on the patient couch, as close as possible to the gantry, such that the back surface of the collimator was at a distance of 85.0 cm from the source. The distance was measured with the help of optical distance indicator (ODI) of the linac and a ruler. The patient couch was aligned so that the axis of the beam passed through the center of the collimator's aperture.

The PTW 31014-000959 ionization chamber was placed on the axis of the beam, at a fixed distance of 150 cm from the source throughout the experiment. The radiation sensitive area of the ion chamber was placed on the axis of the beam as shown in Figure 3.11. The ionization chamber was connected with a triaxial cable

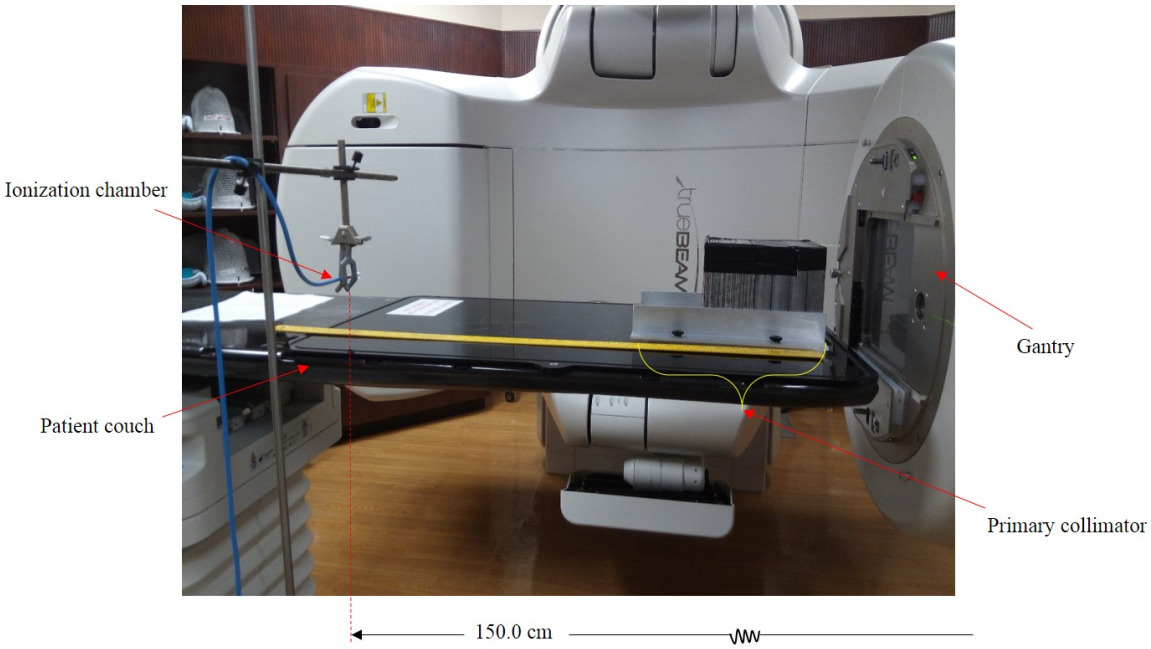

Figure 3.10: Experimental setup to measure the amount of charge created in the sensitive area of an ionization chamber by collimated x-ray beam as a function of the distance from the source to the back surface of the collimator.

to the FLUKE 35040-1568043 electrometer placed in the control room and a biasing voltage of +300 V in the ionization chamber was supplied by the electrometer. The stand that held the ionization chamber was placed on the floor so that the patient couch and hence the primary collimator could be moved independently along the beam's axis, from the control room.

(D) Measurement with 6 MVp x-ray beam

With the primary collimator at its closest distance from the gantry, the 6 MVp x-ray beam was turned ON with field size 10 cm $\times$ 10 cm at a distance of 100 cm from the source and dose per irradiation of 200 MU. A monitor unit (MU) is a measure of machine output, which correlates with a dose of 1 cGy delivered to a water phantom under reference conditions, specific to the linac machine, and it is measured by monitor

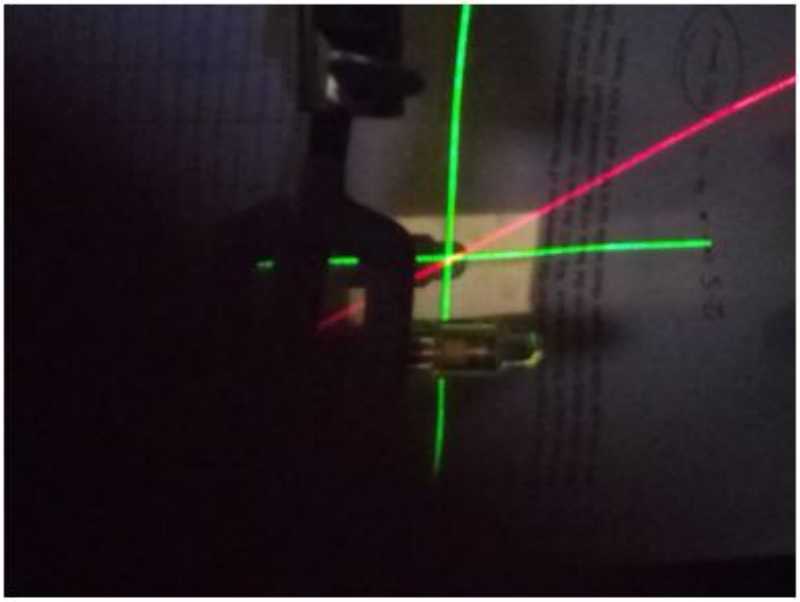

Figure 3.11: Positioning of the the radiation sensitive region of ionization chamber on the axis of beam.

ionization chambers built into the treatment head of radiotherapy linacs. The amount of charge collected by the ionization chamber was recorded from the electrometer. The measurement was repeated two more times at the same position of the primary collimator.

Then the primary collimator was moved towards the ionization chamber by 1 cm so that the distance from the source to the back surface of the collimator was 86.0 cm. With the same beam specification, the ionization chamber was irradiated three times and the amount of charge collected in the ionization chamber was recorded from the electrometer.

This process was repeated until the collimator could reach as close as possible to the ionization chamber. However the increment of the distances by which the collimator was moved towards the ionization chamber could not be maintained con-

Table 3.5: Amount of charge collected by an ionization chamber, placed at 150 cm from the source, as a function of the distance from the source to the back surface of the primary collimator (x).

Distance x(cm)	Charge Q_1 (nC)	Charge Q_2 (nC)	Charge Q_3 (nC)	Average (nC)	Std dev (nC)
85	0.2658	0.2657	0.2659	0.2658	0.0001
86	0.2658	0.2660	0.2659	0.2659	0.0001
87	0.2659	0.2661	0.2660	0.2660	0.0001
89	0.2662	0.2662	0.2662	0.2662	0.0000
91	0.2662	0.2663	0.2664	0.2663	0.0001
96	0.2668	0.2668	0.2670	0.2669	0.0001
101	0.2672	0.2674	0.2673	0.2673	0.0001
106	0.2677	0.2677	0.2631	0.2662	0.0027
111	0.2682	0.2683	0.2682	0.2682	0.0001
121	0.2688	0.2689	0.2690	0.2689	0.0001
131	0.2695	0.2696	0.2696	0.2696	0.0001
141	0.2723	0.2726	0.2724	0.2724	0.0002
144	0.2754	0.2755	0.2757	0.2755	0.0002

stant because of the beam time limitation. Due to the blockage by the clamp that held ionization chamber, the ionization chamber could not be moved closer than 6 cm from the ionization chamber. Table 3.5 shows the amount of charge collected by the ionization chamber placed at a fixed distance of 150 cm from the source as a function of the distance from the source to the back surface of the primary collimator, with 6 MVp x-ray beam.

The standard deviation of the three consecutive measurements taken in each position of the collimator was calculated in table 3.5 using:

$$\sigma = \sqrt{\frac{\sum_{i=1}^{n}(Q_i - Q_o)^2}{n-1}}, \tag{3.3}$$

where n is the number of measurements in a specific position of the collimator, $\{Q_1$, Q_2, ..., $Q_n\}$ are the measured values, and Q_o is the average of all these measured values.

(E) Measurement with 10 MVp x-ray beam

After taking the measurements using the 6 MVp x-ray beam, the primary collimator was brought to its closest position from the gantry so that the distance from the source to the back surface of the primary collimator was 85.0 cm. Then the ionization chamber was irradiated with the 10 MVp x-ray beam. The field size of the beam was chosen to be 10 cm $\times$ 10 cm at a distance of 100 cm from the source. The amount of dose requested in each irradiation was 200 MU.

Table 3.6: Amount of charge collected by an ionization chamber, placed at 150 cm from the source, as a function of the distance from the source to the back surface of the primary collimator (x), with 10 MVp x-ray beam.

Distance x(cm)	Charge Q_1 (nC)	Charge Q_2 (nC)	Charge Q_3 (nC)	Average (nC)	Std dev (nC)
85	193.87	193.91	194.13	193.97	0.14
86	194.05	193.96	193.94	193.98	0.06
87	194.11	194.07	193.94	194.04	0.09
89	194.32	194.34	194.27	194.31	0.04
91	194.41	194.39	194.45	194.42	0.03
96	194.89	194.94	194.88	194.90	0.03
101	195.47	195.48	195.35	195.43	0.07
106	196.02	196.17	196.22	196.14	0.10
111	196.70	196.63	196.62	196.65	0.04
121	197.77	197.82	197.80	197.80	0.03
131	199.26	199.27	199.20	199.24	0.04
141	205.10	205.20	205.20	205.17	0.06
144	211.10	211.10	211.00	211.07	0.06

The primary collimator was moved towards the ionization chamber by 1.0 cm and the ionization chamber was irradiated with the same beam three different times. In the same way, the measurements were taken with the 10 MVp x-ray beam with the primary collimator placed at various distances (x) from the source, as listed in table 3.6. Table 3.6 also summarizes the amount of charge created by the collimated beam in the ionization chamber at each position of the primary collimator. The standard deviation listed on 6^{th} column was calculated using equation 3.3.

3.3.2 Assessment of the contamination from characteristic x-rays produced by the aperture of the primary collimator

(A) Purpose:

The goal of this experiment was to (i) measure the relative amount of characteristic x-rays produced from the inner surface of the primary collimator's aperture as a function of the distance between the source and the primary collimator, and (ii) to determine the necessity of the copper filter in the primary collimator.

(B) Equipment:

The Varian TrueBeam linear accelerator (model number: 1200), described in section 3.3.1(B), was used as the source of x-ray beams. X-ray beams with two different nominal energies, 6 and 10 MVp, were used in the measurement. The PTW pinpoint ionization chamber of type number 31014 and serial number 000959, connected to the Fluke 35040 Advanced Therapy Dosimeter (ATD), explained in section 3.3.1(B), was used as the detector.

(C) Experimental setup

Figure 3.12 shows the setup that was used for this experiment. The gantry of the linac was set at 90^o relative to a vertical axis which provided horizontal x-ray beams. The primary collimator was placed on the patient couch, very close to the gantry, such that the back surface of the collimator was at a distance of 80.8 cm from the source. The patient couch and the collimator were aligned to make the axis of the

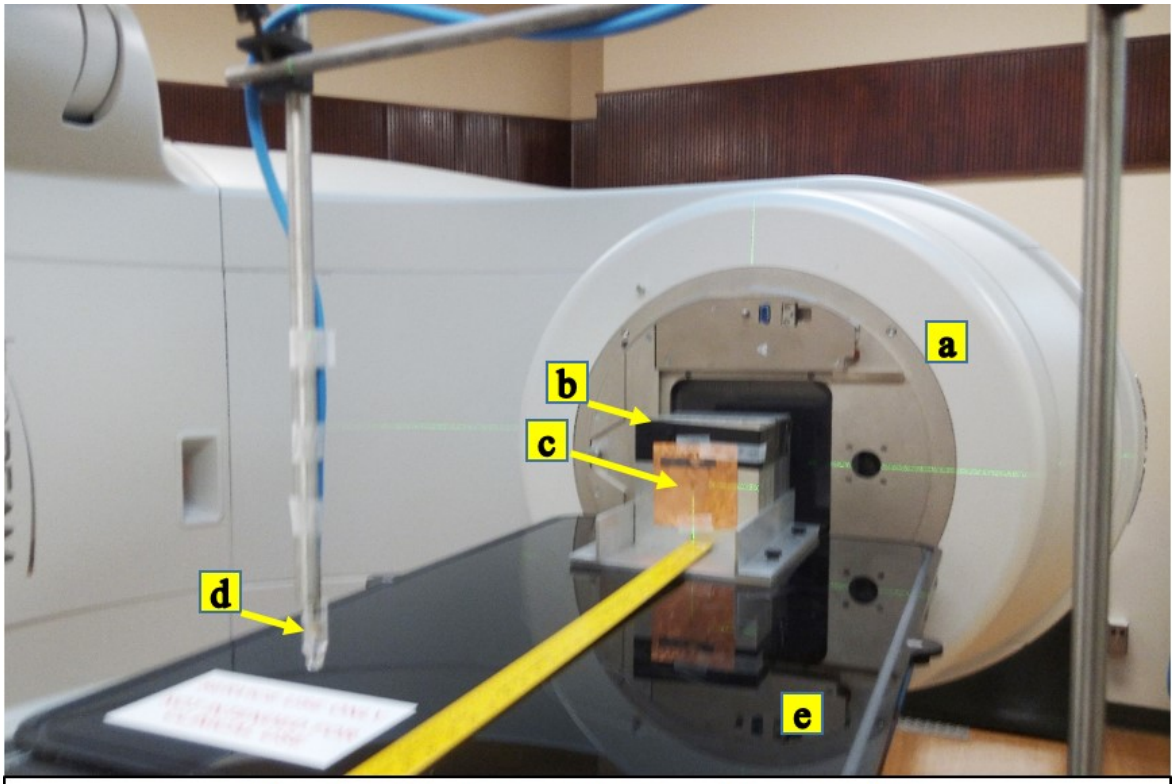

(a) gantry, (b) primary collimator, (c) copper filter
(d) ionization chamber, (e) patient couch

Figure 3.12: Experimental setup for the assessment of the contamination from characteristic x-rays produced by the aperture of the primary collimator.

beam pass through the center of the collimator's aperture.

The PTW 31014-000959 ionization chamber was placed on the axis of the beam, at a fixed distance of 150 cm from the source throughout the experiment. Its radiation sensitive area was centered on the beam's axis, as shown in Figure 3.13. The ionization chamber was connected using a triaxial cable to the FLUKE 35040-1568043electrometer electrometer, placed in the control room. A biasing voltage of +300 V was supplied to the ionization chamber from the electrometer.

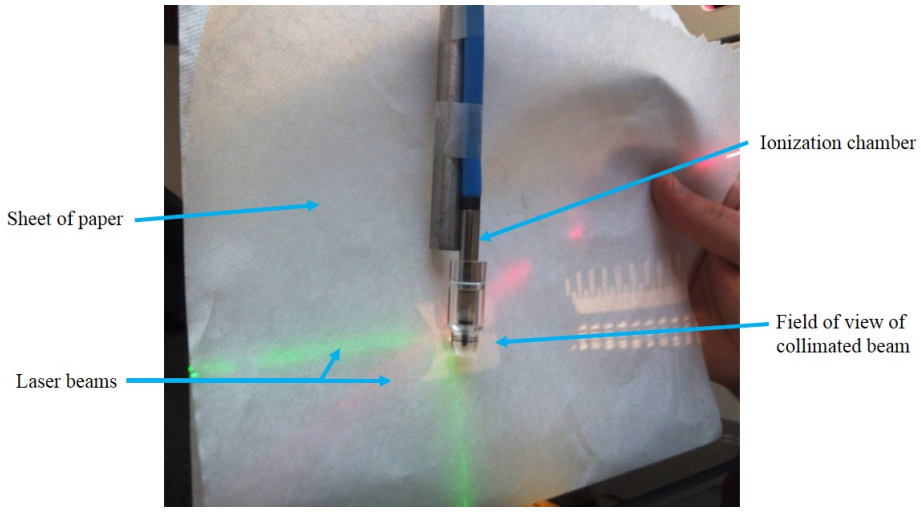

Figure 3.13: Positioning the radiation sensitive area of ionization chamber on the axis of the beam with the help of laser beams.

(D) Measurement without using the copper filter in the primary collimator

The copper filter was removed from the primary collimator. The 6 MVp x-ray beam from the linac was used to irradiate the ionization chamber. The field size of the beam was requested to be 10×10 cm^2 at a distance of 100 cm from the source. The dose per irradiation was 200 MU which was delivered by the linac in about 20 s, at the rate of 600 Gy/min. The amount of charge collected in the sensitive area of the ionization chamber was recorded from the electrometer. The measurement was repeated one more time in the same position of the primary collimator.

Then the primary collimator was moved along the beam's axis by 5 cm towards the ionization chamber so that the distance to the back surface of the primary collimator from the ionization chamber was 64.2 cm, i.e. 85.8 cm from the source. The ionization chamber was irradiated by the 6 MVp beam with the same specification as used in the previous irradiation. The amount of charge collected in two separate measurements were recorded from the electrometer.

Table 3.7: Amount of charge collected by the ionization chamber, as a function of the distance (x) from the source to the back surface of the primary collimator. The ionization chamber was irradiated with the 6 MVp x-ray beam that was collimated by the primary collimator in the absence of copper filter.

Distance x(cm)	Charge Q_1 (nC)	Charge Q_2 (nC)	Average (nC)	Std dev (nC)
80.8	0.2692	0.2694	0.2693	0.0001
85.8	0.2694	0.2694	0.2694	0.0000
90.8	0.2697	0.2697	0.2697	0.0000
95.8	0.2704	0.2704	0.2704	0.0000
100.8	0.2710	0.2710	0.2710	0.0000
105.8	0.2712	0.2713	0.2713	0.0001
110.8	0.2712	0.2711	0.2712	0.0001
115.8	0.2705	0.2707	0.2706	0.0001
120.8	0.2697	0.2696	0.2697	0.0001
125.8	0.2683	0.2683	0.2683	0.0000
130.8	0.2665	0.2665	0.2665	0.0000
135.8	0.2649	0.2648	0.2649	0.0001
140.8	0.2635	0.2636	0.2636	0.0001
145.8	0.2676	0.2679	0.2678	0.0002

With the increment of 5 cm, the primary collimator was moved towards the ionization chamber. And the measurements were taken at each position of the collimator in the similar way. The measured values of the charge with the primary collimator placed at various distances from the source are summarized in Table 3.7. The values of the standard deviation listed in last column were calculated using equation 3.3.

After taking the measurements with 6 MVp x-ray beam, the primary collimator was brought to its nearest position from the gantry and the measurements were repeated with the 10 MVp x-ray beam. The field size and the dose per exposure in the beam were chosen to be same as in the measurement with 6 MVp beam. The primary collimator was placed in exactly the same positions as listed in table 3.7. The measured values of the charge using 10 MVp x-ray beam with the primary collimator placed at various distances from the source, are summarized in Table 3.8. The values

Table 3.8: Amount of charge collected by the ionization chamber, as a function of the distance (x) from the source to the back surface of the primary collimator. The ionization chamber was irradiated with the 10 MVp x-ray beam that was collimated by the primary collimator in the absence of copper filter.

Distance x(cm)	Charge Q_1 (nC)	Charge Q_2 (nC)	Average (nC)	Std dev (nC)
80.8	0.2007	0.2007	0.2007	0.0000
85.8	0.2008	0.2008	0.2008	0.0000
90.8	0.2013	0.2014	0.2014	0.0001
95.8	0.2022	0.2024	0.2023	0.0001
100.8	0.2034	0.2032	0.2033	0.0001
105.8	0.2038	0.2037	0.2038	0.0001
110.8	0.2039	0.2040	0.2040	0.0001
115.8	0.2036	0.2036	0.2036	0.0000
120.8	0.2031	0.2029	0.2030	0.0001
125.8	0.2020	0.2020	0.2020	0.0000
130.8	0.2012	0.2012	0.2012	0.0000
135.8	0.2009	0.2009	0.2009	0.0000
140.8	0.2030	0.2030	0.2030	0.0000
145.8	0.2157	0.2157	0.2157	0.0000

of the standard deviation listed in last column were calculated using equation 3.3.

(E) Measurement using the copper filter in the primary collimator

The copper filter was put back on the primary collimator and the collimator was brought nearest to the gantry, such that the distance between the source and the back surface of the collimator was 80.8 cm. The ionization chamber was placed at the same position as in the previous setup. Using the 6 MVp x-ray beam with the field size of 10 cm $\times$ 10 cm at a distance of 100 cm from the source and a dose per irradiation of 200 MU, the ionization chamber was irradiated with the collimator placed at various distances from the source. The measured values of the charge by the ionization chamber as a function of the source to collimator distance are summarized in table 3.9.

Table 3.9: Amount of charge collected by the ionization chamber, as a function of the distance (x) from the source to the back surface of the primary collimator. The ionization chamber was irradiated with the 6 MVp x-ray beam that was collimated by the primary collimator in the presence of copper filter.

Distance x(cm)	Charge Q_1 (nC)	Charge Q_2 (nC)	Charge Q_3 (nC)	Average (nC)	Std dev (nC)
80.8	0.2744	0.2743	0.2744	0.2744	0.0001
85.8	0.2746	0.2746	0.2746	0.2746	0.0000
90.8	0.2745	0.2744	0.2746	0.2745	0.0001
95.8	0.2748	0.2748	0.2750	0.2749	0.0001
100.8	0.2756	0.2754	0.2755	0.2755	0.0001
105.8	0.2760	0.2760	0.2762	0.2761	0.0001
110.8	0.2762	0.2763	0.2763	0.2763	0.0001
115.8	0.2767	0.2765	0.2766	0.2766	0.0001
120.8	0.2768	0.2769	0.2769	0.2769	0.0001
125.8	0.2772	0.2772	0.2771	0.2772	0.0001
130.8	0.2775	0.2775	0.2776	0.2775	0.0001
135.8	0.2783	0.2784	0.2784	0.2784	0.0001
140.8	0.2807	0.2806	0.2800	0.2804	0.0004
145.8	0.2913	0.2914	0.2916	0.2914	0.0002

Then the measurements were repeated with the 10 MVp x-ray beam by putting the primary collimator at the same positions as listed in table 3.9. All the beam properties for each irradiation was same as in the previous irradiations. The measured values of the charge by the ionization chamber as a function of the source to collimator distance are summarized in table 3.10. The values of the standard deviation listed in last column were calculated using equation 3.3.

Table 3.10: Amount of charge collected by the ionization chamber, as a function of the distance (x) from the source to the back surface of the primary collimator. The ionization chamber was irradiated with the 6 MVp x-ray beam that was collimated by the primary collimator in the presence of copper filter.

Distance x(cm)	Charge Q_1 (nC)	Charge Q_2 (nC)	Average (nC)	Std dev (nC)
80.8	0.1994	0.1994	0.1994	0.0000
85.8	0.1994	0.1995	0.1995	0.0001
90.8	0.1998	0.1998	0.1998	0.0000
95.8	0.2007	0.2008	0.2008	0.0001
100.8	0.2018	0.2016	0.2017	0.0001
105.8	0.2021	0.2022	0.2022	0.0001
110.8	0.2022	0.2022	0.2022	0.0000
115.8	0.2019	0.2019	0.2019	0.0000
120.8	0.2012	0.2013	0.2013	0.0001
125.8	0.2004	0.2002	0.2003	0.0001
130.8	0.1993	0.1993	0.1993	0.0000
135.8	0.1988	0.1986	0.1987	0.0002
140.8	0.2016	0.2015	0.2016	0.0001
145.8	0.2179	0.2180	0.2180	0.0001

3.3.3 Radial distribution of the intensity of the collimated beam by the primary collimator

(A) Purpose

The goal of this experiment was to measure the radial distribution of the intensity of the collimated x-ray beam by the primary collimator at a given distance from the source while putting the primary collimator at its optimal position, determined by the previous two experiments (sections 3.3.1 and 3.3.2).

(B) Equipment

The Varian TrueBeam linear accelerator (model number: 1200), described in section 3.3.1(B), was used as the source of x-ray beams. The measurements were

taken only with the 6 MVp x-ray beam from the linac. The PTW pinpoint ionization chamber of type number 31014 and serial number 000959, connected to the Fluke 35040 Advanced Therapy Dosimeter (ATD), explained in section 3.3.1(B), was used as the detector.

A ruler, taped on a stand was used to measure the positions of ionization chamber across the vertical field of view. A plumb bob pointing to a horizontal ruler was used to measure the relative positions of the ionization chamber across the horizontal field of view.

(C) Experimental setup

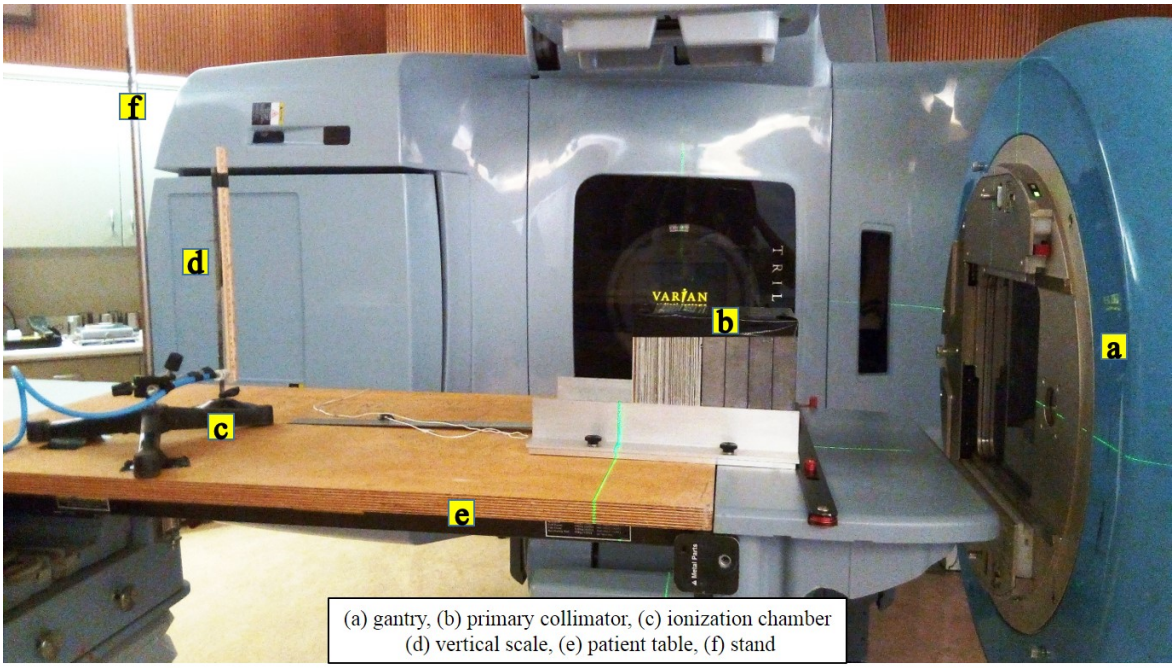

Figure 3.14: Experimental setup for the measurement of the radial distribution of the beam beyond the primary collimator.

Figure 3.14 shows the experimental setup used in this experiment. The gantry was set at 90^o relative to a vertical axis which provided horizontal x-ray beams from the linac. The primary collimator was placed on the patient couch and was

aligned in such a way that the axis of the beam passed through the center of the collimator.

The PTW 31014-000958 ionization chamber was placed on the axis of the beam, at a distance of 150 cm from the source. The ionization chamber was connected with a triaxial cable to the FLUKE 35040 electrometer, located in the control room.

The position of primary collimator was determined based on the amount of charge measured by an ionization chamber placed at 150 cm from the source as a function of the distance from the source to the primary collimator, in previous two experiments. As seen in tables 3.5 – 3.10, the primary collimator minimizes the secondary x-rays at 150 cm from the source when the distance between the source and the back surface of the primary collimator is in between 80 cm and 100 cm. The distance to the back surface of the primary collimator from the ionization chamber was therefore fixed to be 53 cm, i.e. 97 cm from the source.

(D) Measurement of radial intensity distribution across vertical field

Figure 3.15 shows a schematic diagram (not in scale) of the field of view of x-ray beam collimated by the primary collimator. The ionization chamber was first placed at a point, A, outside the field of view. The point A was considered as a reference point from which the distance of ionization chamber placed at various points along the line AB were measured. The 6 MVp x-ray beam with the field size of 10 cm $\times$ 10 cm at a distance of 100 cm from the source was used to irradiate the ionization chamber at the reference point. The dose per irradiation was requested to be 200 MU.

Then the ionization chamber was moved by 0.4 cm towards the axis and was irradiated by using the same beam. Similarly, the ionization chamber was placed at various distances from the reference point, listed in table 3.11, along the line AB and

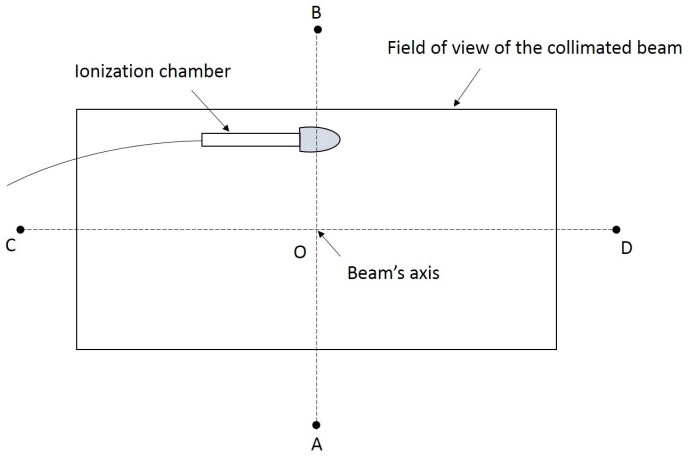

Figure 3.15: Schematic diagram illustrating the field of view of the x-ray beam collimated by the primary collimator. To measure the radial intensity distribution in vertical direction, the ionization chamber was placed at various points along the line AB. And for the radial distribution of the intensity in the horizontal direction, the ionization chamber was placed at various points along line CD.

was irradiated with x-ray beams. The position of ionization chamber was measured with the help of a vertical ruler attached to a stand. The stand was taken away while the beam was ON to prevent from any secondary x-rays produced in the stand that reach the ionization chamber. Table 3.11 summarizes the amount of charge that the ionization chamber collected, recorded from the electrometer, in each position across vertical field of view. The values of the standard deviation listed in last column were calculated using equation 3.3.

(E) Measurement of radial intensity distribution across horizontal field

The ionization chamber was placed at a point, C, outside the field of view. The point C was considered as a reference point from which the distance to the ionization chamber placed at various points along the line CD were measured. The ionization chamber at its reference point was irradiated with the 6 MVp x-ray beam. The beam

Table 3.11: Amount of charge collected in the ionization chamber due to the collimated x-ray beam as a function of the ion-chamber's position along the vertical field of view.

Position of ionization chamber (cm)	Charge Q_1 (nC)	Charge Q_2 (nC)	Average (nC)	Std dev (nC)
0	0.0178	0.0171	0.0174	0.0005
0.4	0.2300	0.2302	0.2301	0.0001
0.8	0.2546	0.2539	0.2543	0.0005
1.2	0.2570	0.2562	0.2566	0.0006
1.9	0.2560	0.2564	0.2562	0.0003
2.3	0.2369	0.2359	0.2364	0.0007
2.7	0.0275	0.0268	0.0272	0.0005

properties for each exposure were kept same as in the measurements along the line AB.

Table 3.12: Amount of charge collected in the ionization chamber due to the collimated x-ray beam as a function of the ion-chamber's position along the horizontal field of view.

Position of ionization chamber (cm)	Charge Q_1 (nC)	Charge Q_2 (nC)	Average (nC)	Std dev (nC)
0	0.0406	0.0401	0.0404	0.0004
0.5	0.2482	0.2473	0.2478	0.0006
1.1	0.2584	0.2575	0.2580	0.0006
1.5	0.2580	0.2572	0.2576	0.0006
1.8	0.2582	0.2572	0.2577	0.0007
2.2	0.2588	0.2578	0.2583	0.0007
2.6	0.2590	0.2588	0.2589	0.0001
3.0	0.2600	0.2596	0.2598	0.0003
3.4	0.2608	0.2603	0.2606	0.0004
3.9	0.2618	0.2615	0.2617	0.0002
4.2	0.2620	0.2621	0.2621	0.0001
4.5	0.2608	0.2613	0.2611	0.0004
4.8	0.2528	0.2524	0.2526	0.0003
5.1	0.0525	0.0521	0.0523	0.0003

The ionization chamber was moved by 0.5 cm towards the beam's axis and was irradiated. Similarly, the ionization chamber was placed at various distances listed in table 3.12 from the reference point (C), along the line CD. To measure the relative

relative position of the ionization chamber, a plum bob pointing to a horizontal ruler placed on table, underneath the ionization chamber, was used. Table 3.12 summarizes the amount of charge that the the ionization chamber collected at each position of the ionization chamber across the horizontal field of view. The values of the standard deviation listed in last column were calculated using equation 3.3.

3.3.4 Radial distribution of the intensity of attenuated x-ray beam by an absorber at a given distance from the source

(A) Purpose

The purpose of this experiment was to measure the radial distribution of the intensity of attenuated x-ray beam by an absorber.

(B) Equipment

The Varian TrueBeam linear accelerator (model number: 1200), described in section 3.3.1(B), was used as the source of x-ray beams. The measurements were taken only with the 6 MVp x-ray beam. The PTW pinpoint ionization chamber of type number 31014 and serial number 000959, connected to the Fluke 35040 Advanced Therapy Dosimeter (ATD), explained in section 3.3.1(B), was used as the detector.

A ruler, taped on a stand was used to measure the positions of ionization chamber across the vertical field of view. A plumb bob pointing to a horizontal ruler was used to measure the relative positions of the ionization chamber across the horizontal field of view.

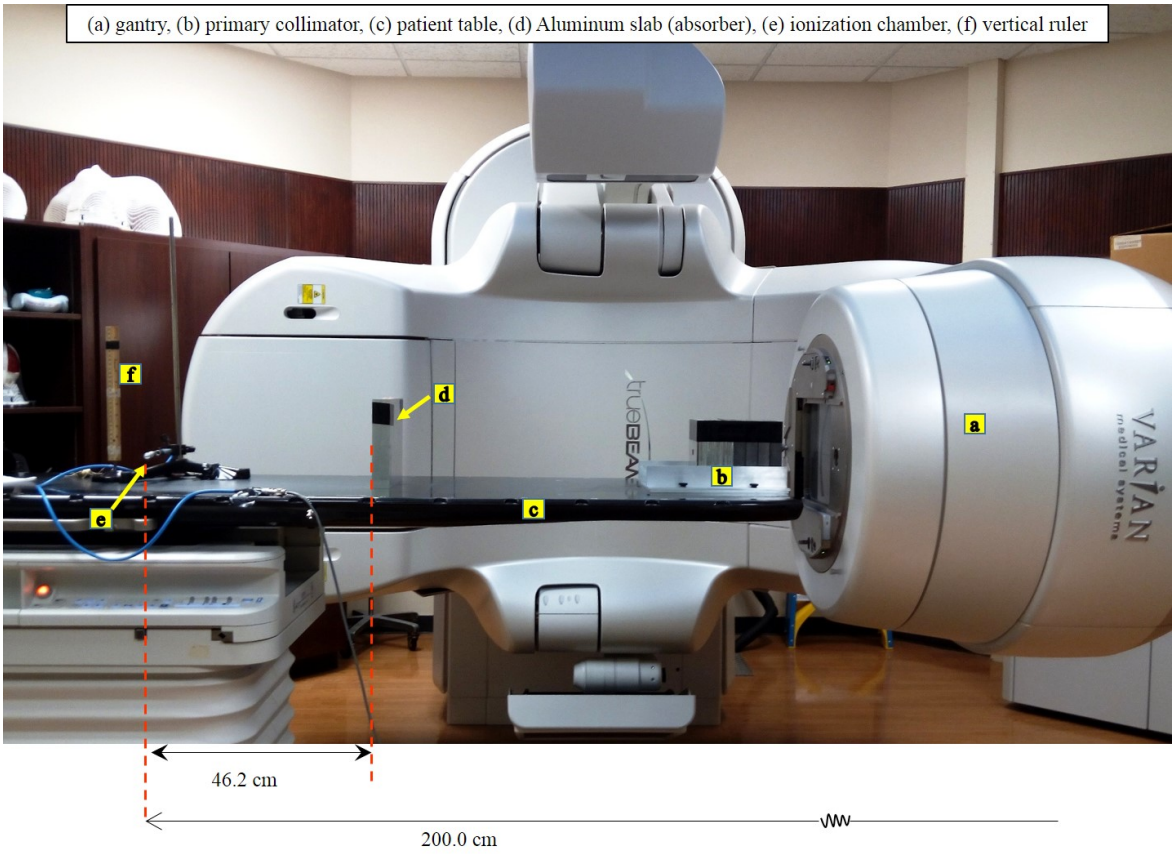

Figure 3.16: Experimental setup for the measurement of the radial distribution of the intensity of the beam beyond the absorber.

(C) Experimental setup

Figure 3.16 shows the experimental setup used in this experiment. The gantry was set at 90° relative to a vertical axis which provided horizontal x-ray beams from the machine. The position of the primary collimator was decided based on the experiments presented in sections 3.3.1 and 3.3.2 so that it could sufficiently collimate the x-ray beam to the position of the absorber, placed at 150 cm from the source. The distance from the source to the back surface of the primary collimator was made to be 83.8 cm. The primary collimator and the patient couch were aligned to make the beam's axis pass through the center of the collimator's aperture. The position of the primary collimator was fixed throughout the measurement.

The PTW 31014-000959 ionization chamber was placed at a distance of 200 cm from the source such that the radiation sensitive area of the chamber was on the beam's axis. It was connected with a triaxial cable to the FLUKE 35040-1568043 electrometer placed in the control room and a biasing voltage of +300 V in the chamber was supplied by the electrometer.

At a distance of 150 cm from the source, two slabs of aluminum with the total thickness of 3.68 cm were placed so that the x-ray beam, collimated by the primary collimator, was attenuated before reaching the ionization chamber.

(D) Measurement of radial intensity distribution across vertical field

Figure 3.15 illustrates a possible shape of the field of view of the beam attenuated by the absorber. By keeping the longitudinal distance from the source to the ionization chamber fixed at 200 cm, the ionization chamber was first placed to a point, A, outside the field of view and underneath the beam's axis as shown in Figure 3.15. That position was taken as a reference point (0 cm) with respect to which the distances of ionization chamber at various points along the line AB, were measured.

Table 3.13: Amount of charge collected by the ionization chamber due to the 6 MVp x-ray beam, attenuated by an absorber, as a function of the ion-chamber's position across the vertical field of view.

Position of ionization chamber (cm)	Charge Q_1 (pC)	Charge Q_2 (pC)	Average (pC)	Std dev (pC)
0	8.72	9.24	8.98	0.37
0.5	67.11	66.83	66.97	0.20
1	91.23	92.01	91.62	0.55
1.5	91.87	91.79	91.83	0.06
2.5	91.80	91.83	91.82	0.02
3.5	91.32	91.39	91.36	0.05
3.8	90.51	90.52	90.52	0.01
4	71.92	71.86	71.89	0.04
4.5	7.77	7.83	7.80	0.04

The 6 MVp x-ray beam with the field size of 10 cm $\times$ 10 cm at a distance of 100 cm from the source was used to irradiate the ionization chamber at the reference point. The dose requested in a single irradiation was 200 MU. Then the ionization chamber was moved by 0.5 cm above the reference point and was irradiated by x-ray beam. This process was continued until the ionization chamber was outside the beam's field of view. At each position, two measurements were taken.

The relative position of the ionization chamber was measured with the help of a vertical ruler attached to a stand. The stand was taken away while the beam was ON to prevent from any secondary x-rays produced in the stand that reach the ionization chamber. Table 3.13 summarizes the measured charge with the ionization chamber placed at various points across the vertical field of view. The values of the standard deviation listed in last column were calculated using equation 3.3.

(E) Measurement of radial intensity distribution across horizontal field

The ionization chamber was placed at a point, C, outside the beam's field of view, on line CD in Figure 3.15 and was irradiated with the 6 MVp x-ray beam. Other beam properties such as the field size and the monitor unit for each exposure were chosen to be same as in the previous irradiation.

After taking two separate measurements with the ionization chamber placed on the reference point (0 cm), the ionization chamber was moved by 1 cm towards the beam's axis. A plumb bob pointing to a horizontal ruler, placed underneath the ionization chamber on the table, was used to measure the relative position of the ionization chamber from the reference point. Similarly, the ionization chamber was moved by an incremental distance of 1 cm until the ionization chamber was outside the field of view (D). At each position the ionization chamber was irradiated with

Table 3.14: Amount of charge collected by the ionization chamber due to the 6 MVp x-ray beam, attenuated by an absorber, as a function of the ion-chamber's position across the horizontal field of view.

Position of ionization chamber (cm)	Charge Q_1 (pC)	Charge Q_2 (pC)	Average (pC)	Std dev (pC)
0.0	32.78	32.83	32.805	0.04
1.0	95.29	95.4	95.345	0.08
1.5	95.43	95.45	95.44	0.01
2.5	95.74	95.7	95.72	0.03
3.5	95.75	95.64	95.695	0.08
4.5	95.64	95.6	95.62	0.03
5.5	95.43	95.31	95.37	0.08
6.5	94.84	94.73	94.785	0.08
7.5	18.41	18.32	18.365	0.06
8.5	3.1	3.02	3.06	0.06

the 6 MVp beam and corresponding readings for the charge were recorded from the electrometer. Table 3.14 summarizes the amount of charge that the the ionization chamber collected at various positions across the horizontal field of view. The values of the standard deviation listed in last column were calculated using equation 3.3.

3.3.5 Determination of the optimal position of the secondary collimator

(A) Purpose

The purpose of this experiment was to determine an optimal position for the secondary collimator at which the collimator can (i) sufficiently collimate the x-ray beam attenuated by an absorber, and (ii) minimize the secondary x-rays, produced by the absorber and the secondary collimator itself, that reach to the detector placed at a given distance from the absorber.

(B) Equipment

The Trilogy linear accelerator (model number: 1200), manufactured by Varian Medical Systems Inc, was used as the source of x-ray beams in this experiment. The Varian Trilogy is an isocentric unit capable of producing photon beam with nominal energies of 6 MVp and 18 MVp. It also produces electron beams with five different energies: 6, 9, 12, 16, and 20 MeV. The collimators were mounted on the couch, used for patient positioning during radiotherapy and radiosurgery procedures.

The PTW pinpoint ionization chamber of type number 31014 and serial number 000958, connected to the Fluke 35040 Advanced Therapy Dosimeter (ATD), explained in section 3.3.1(B), was used as the detector. Aluminum slabs with total thickness of 3.68 cm was used as absorber.

(C) Experimental setup

Figure 3.17 shows the experimental setup used in this experiment. The gantry of the linac was set at 90^{o} relative to a vertical axis which provided horizontal x-ray beams from the machine. The primary collimator was placed on the top of the patient couch and was aligned so that the beam's axis passed through the center of its aperture. The distance from the source to the back surface of the primary collimator was made to be 97 cm. The position of the primary collimator was fixed throughout the experiment.

The PTW 31014-000959 ionization chamber was placed at a fixed distance of 200 cm from the source such that the radiation sensitive area of the chamber was always on the beam's axis. It was connected with a triaxial cable to the FLUKE 35040-1568043 electrometer placed in the control room and a biasing voltage of +300

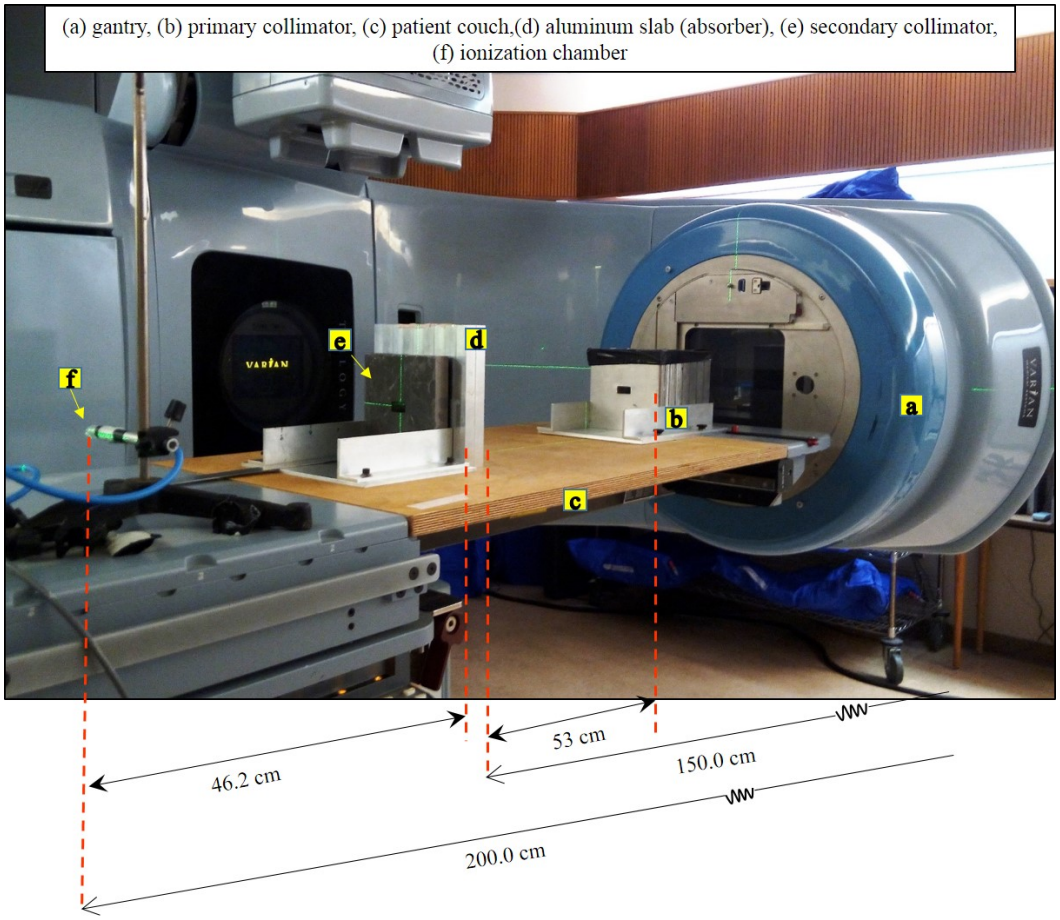

Figure 3.17: Experimental setup for the determination of an optimal position of the secondary collimator.

V in the chamber was supplied by the electrometer.

A 3.68 cm thick aluminum absorber was placed at a distance of 150 cm from the source. The secondary collimator was placed behind the absorber and was aligned with the primary collimator.

(D) Measurement

The secondary collimator was placed very close to the absorber such that the back surface of the secondary collimator was 45.0 cm away from the ionization

chamber, i.e. 155.0 cm from the source. Then the ionization chamber was irradiated with the 6 MVp x-ray beam with the field size of 10 cm $\times$ 10 cm at a distance of 100 cm from the source. The dose requested for a single irradiation was 200 MU. The amount of charge collected by the ionization chamber was recorded from the electrometer. The measurement was repeated at the same position of the secondary collimator.

Table 3.15: Amount of charge measured by ionization chamber as a function of the distance (x) between the source and the back surface of the collimator

Distance x (cm)	Charge Q_1 (pC)	Charge Q_2 (pC)	Average (pC)	Std dev (pC)
155.0	87.65	87.65	87.65	0.00
160.0	88.63	87.82	88.23	0.57
165.0	88.83	87.83	88.33	0.71
170.0	89.15	85.19	87.17	2.80
175.0	88.91	88.08	88.50	0.59
180.0	90.85	90.31	90.58	0.38
185.0	89.68	89.41	89.55	0.19
190.0	91.16	90.95	91.06	0.15

By keeping all other components at the same position, the secondary collimator was moved by 5.0 cm towards the ionization chamber and the measurement was repeated. Similarly, the the measurements were taken at various positions of the secondary collimator, in between the absorber and the ionization chamber. The alignment of the secondary collimator at each position was carefully checked before irradiation. Table 3.15 summarizes all the measured charges with the secondary collimator placed at various positions. The values of the standard deviation listed in last column were calculated using equation 3.3.

3.3.6 Radial distribution of the collimated beam beyond the secondary collimator

(A) Purpose

The purpose of this experiment was to determine the radial distribution of the intensity of an x-ray beam at the position of detector while measuring attenuation data by keeping the primary and secondary collimators in their respective optimal positions.

(B) Equipment

The Varian TrueBeam linear accelerator (model number: 1200), described in section 3.3.1(B), was used as the source of x-ray beams. The measurements were taken only with the 6 MVp x-ray beam from the linac. The PTW pinpoint ionization chamber of type number 31014 and serial number 000959, connected to the Fluke 35040 Advanced Therapy Dosimeter (ATD), explained in section 3.3.1(B), was used as the detector.

A ruler, taped on a stand was used to measure the positions of ionization chamber across the vertical field of view. A plumb bob system attached with a horizontal ruler was used to measure the relative positions of the ionization chamber across the horizontal field of view.

(C) Experimental setup

Figure 3.18 shows the experimental setup of this experiment. The gantry of the linac was set at 90^{o} relative to a vertical axis which provided horizontal x-ray

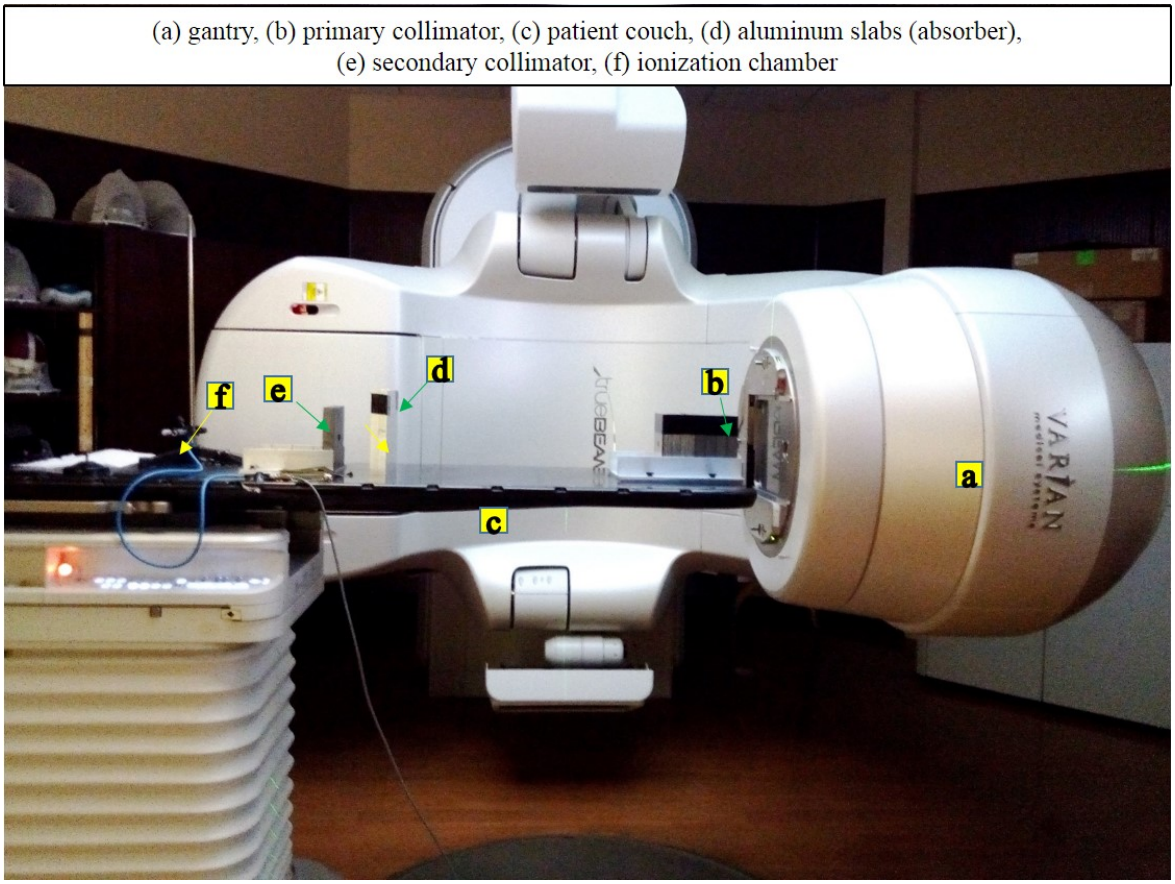

Figure 3.18: Experimental setup for the determination of the radial distribution of the intensity of the beam beyond secondary collimator.

beams. On the top of the patient couch, the PTW TN31014 ionization chamber was placed at a distance of 200 cm from the source.

The primary collimator was placed on the patient couch close to the gantry so that the distance between the source and the back surface of the collimator was 83.8 cm. The position of the primary collimator was chosen based on the result of the experiment presented in sections 3.3.1 and 3.3.2 so that the number of secondaries produced by various components inside the gantry and the primary collimator is minimized at a distance of 150.0 cm from the source. Two slabs of aluminum with a total thickness of 3.67 cm were placed at a distance of 150 cm from the source.

The secondary collimator was placed behind the absorber so that the distance between the back surface of secondary collimator to the ionization chamber was 33.8 cm, i.e. 166.2 cm from the source. The position of the secondary collimator was chosen based on the previous experiment, described in section 4.5, to minimize the secondaries produced by the absorber and the secondary collimator itself that reach the ionization chamber. Both the primary and the secondary collimators were aligned to each other such that the axis of the beam passed through the center of their apertures.

(D) Measurement of radial intensity distribution across vertical field

Figure 3.15 represents the shape of the field of view of the beam collimated by the secondary collimator. By keeping the longitudinal distance from the source to the ionization chamber fixed at 200 cm, the ionization chamber was first placed to a point, A, outside the field of view and underneath the beam's axis. That position was taken as a reference point (0 cm) with respect to which the distances of ionization chamber placed at various points along the line AB, were measured.

Table 3.16: Amount of charge collected by the ionization chamber due to the 6 MVp x-ray beam, attenuated by an absorber, as a function of the ion-chamber's position across the vertical field of view.

Position of ionization chamber (cm)	Charge Q_1 (nC)	Charge Q_2 (pC)	Average (pC)	Std dev (pC)
0	21.36	21.36	21.36	0.00
0.5	68.58	68.68	68.63	0.07
1.0	91.29	91.10	91.20	0.13
1.5	91.50	91.54	91.52	0.03
2.0	90.50	90.61	90.56	0.08
2.3	73.38	73.32	73.35	0.04
2.5	25.71	25.86	25.79	0.11
3.3	22.30	22.11	22.21	0.13

The 6 MVp x-ray beam with the field size of 10 cm $\times$ 10 cm at a distance of 100 cm from the source was used to irradiate the ionization chamber at its reference

position. The dose requested in a single irradiation was 200 MU. Then the ionization chamber was moved by 0.5 cm above the reference point and was irradiated by x-ray beam. This process was continued until the ionization chamber was outside the beam's field of view. At each position, two measurements were taken and the relative position of the ionization chamber was measured with the help of a vertical ruler attached to a stand. The stand was taken away while the beam was ON to prevent from any secondary x-rays produced in the stand that reach the ionization chamber. Table 3.16 summarizes the measured charge with the ionization chamber placed at various points across the vertical field of view. The values of the standard deviation listed in last column were calculated using equation 3.3.

(E) Measurement of radial intensity distribution across horizontal field

Table 3.17: Amount of charge collected in the ionization chamber due to the collimated x-ray beam as a function of the ion-chamber's position along the horizontal field of view.

Position of ionization chamber (cm)	Charge Q_1 (nC)	Charge Q_2 (nC)	Average (nC)	Std dev (nC)
0	22.14	22.15	22.145	0.01
0.5	37.9	37.93	37.915	0.02
1.0	95.36	95.54	95.45	0.13
1.5	95.51	95.63	95.57	0.08
2.0	95.48	95.61	95.545	0.09
2.5	95.54	95.52	95.53	0.01
3.0	95.28	95.39	95.335	0.08
3.5	95.28	95.41	95.345	0.09
3.9	93.99	94.21	94.1	0.16
4.3	52.87	52.87	52.87	0.00
4.7	22.15	22.23	22.19	0.06
5.3	21.78	21.82	21.8	0.03

The ionization chamber was placed at a point C, outside the field of view of the beam as shown in Figure 3.15. That position was taken as a reference position (0 cm) and all other positions of the ionization chamber along the horizontal line CD

were measured from point C. The ionization chamber at its reference position was irradiated by the 6 MVp x-ray beam with the same beam properties same as used in the previous irradiations. A plum bob pointing to a horizontal ruler placed underneath the ionization chamber on the table, was used to measure the relative position of the ionization chamber along CD. Table 3.17 summarizes the amount of charge that the the ionization chamber collected at various positions across the horizontal field of view. The values of the standard deviation listed in last column were calculated using equation 3.3.

Chapter 4

RESULT AND DISCUSSION

4.1 Optimal position of the primary collimator

Table 4.1 summarizes the average charge collected by ionization chamber as a function of the distance from the source to the back surface of the primary collimator, from tables 3.5 and 3.6. The charge collected with the 10 MVp beam are normalized. The normalization was done by multiplying each value of the charge collected with 10 MVp x-ray beam (i.e. column 5 of table 3.6) by the ratio (r) of the charge collected with 6 MVp beam to the charge collected with 10 MVp beam each measured with the primary collimator placed at 85.0 cm from the source. Here, $r = \frac{0.2658}{0.1940} = 1.3703$. The standard deviation in each value of the column 5 in table 3.6 was also normalized by multiplying by r.

The average charge presented in table 4.1 are plotted in Figure 4.1. Here the horizontal axis shows the distance from the source to the back surface of the primary collimator. The error bar in each data point represents the standard deviation in table 4.1 and it has about the same size as the size of the symbol.

As seen from Figure 4.1, the amount of charge collected is almost constant when the distance between the source and the back surface of the collimator is in between 85.0 cm and 100.0 cm. As the primary collimator gets closer to the ionization

Table 4.1: Average charge collected by the ionization chamber using 6 MVp x-ray beam and 10 MVp x-ray beam (normalized) as a function of the distance from the source to the back surface of the primary collimator.

	6 MVp		10 MVp	
distance (cm)	charge (nC)	std. dev. (nC)	charge (nC)	std. dev. (nC)
85.0	0.2658	0.0001	0.2658	0.0002
86.0	0.2659	0.0001	0.2658	0.0001
87.0	0.2660	0.0001	0.2659	0.0001
89.0	0.2662	0.0000	0.2663	0.0000
91.0	0.2663	0.0001	0.2664	0.0000
96.0	0.2669	0.0001	0.2671	0.0000
101.0	0.2673	0.0001	0.2678	0.0001
106.0	0.2662	0.0027	0.2688	0.0001
111.0	0.2682	0.0001	0.2695	0.0001
121.0	0.2689	0.0001	0.2710	0.0000
131.0	0.2696	0.0001	0.2730	0.0001
141.0	0.2724	0.0002	0.2811	0.0001
144.0	0.2755	0.0002	0.2892	0.0001

chamber, the amount of charge collected increases gradually. The increase in charge is possibly due to more number of secondaries produced by the inner surface of the collimator's aperture reach the ionization chamber. This suggests us that the primary collimator should be placed atleast 50 cm away from the ionization chamber, a position that belongs to the plateau region, in order to minimize the number of secondaries produced by the collimator's aperture at the position of ionization chamber which is placed at a distance of 150 cm from the source.

We can also notice that amount of charge (normalized) collected with the 10 MVp x-ray beam is greater than that collected with the 6 MVp beam, specially when the distance between the ionization chamber is less than 50 cm. This means that more number of secondaries are produced from the collimator's aperture with the 10 MVp x-ray beam than the 6 MVp x-ray beam, from this linac.

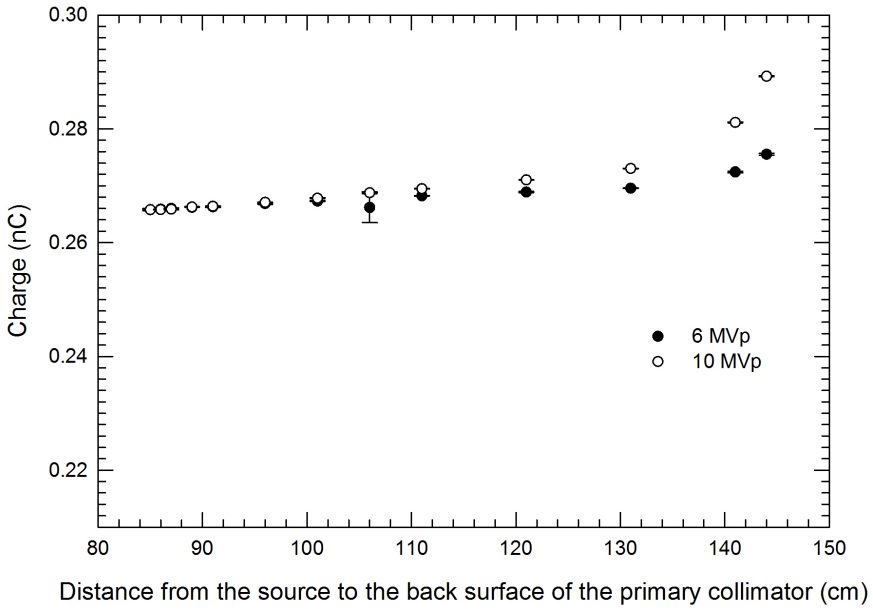

Figure 4.1: Amount of charge collected by the ionization chamber placed at a fixed distance of 150 cm from the source with the primary collimator placed at various positions in between the source and the ionization chamber.

4.2 Characteristic x-rays produced by the aperture of the primary collimator

Figure 4.2 shows a scattered plot of the amount of charge collected by the ionization chamber in the 6 MV beam collimated by the primary collimator, with and without the copper filter on it. The horizontal axis shows the distance from the source to the back surface of the primary collimator. The measured data in the presence of the copper filter is not normalized so that we can see any attenuation of the primary photons that might be caused by the added copper filter. The error bars in the data points represent the standard deviation calculated in tables 3.7 and 3.9. It is hard to see the error bars in the plot because these have about the same size as the size of the symbols.

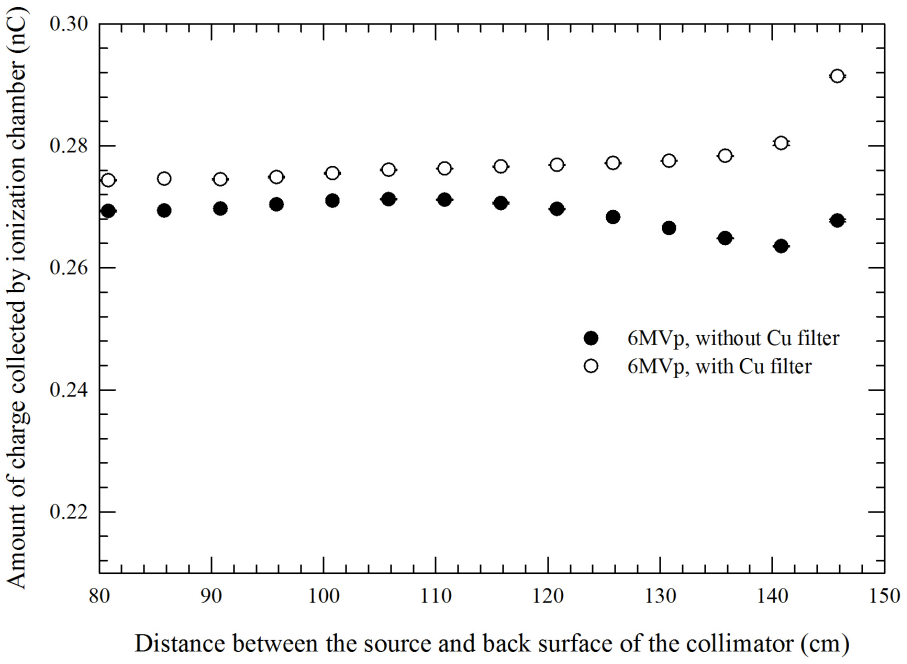

Figure 4.2: Plot of the amount of charge collected by ionization chamber with primary collimator at different positions in between the fixed source and ionization chamber.

Figure 4.3 shows the plot of measured charge using the 10 MVp x-ray beam, collimated by the primary collimator with and without the copper filter on it. The error bars in the data points represent the standard deviation calculated in tables 3.8 and 3.10.

We can see in Figure 4.2 and 4.3 that the measured charge is almost constant with the collimator placed at various distances from the source. When the collimator approaches the ionization chamber the measured charge increases, possibly due to more amount of secondaries reaching the ionization chamber.

In the plateau region of Figure 4.2, the difference between the measured charge with the copper filter and the measured charge without the copper filter is very small. The measured charge in the presence of copper filter is slightly larger than

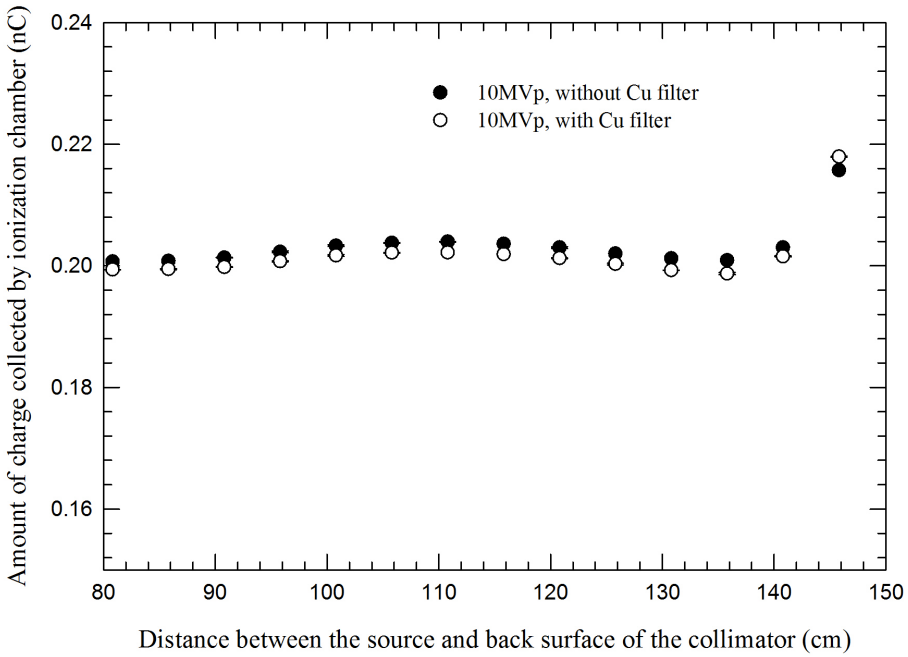

Figure 4.3: Plot of the amount of charge collected by ionization chamber with primary collimator at different positions in between the fixed source and ionization chamber.

that in the absence of copper filter. This indicates that the copper filter does not attenuate the primary x-ray beam but possibly produces some secondaries that reach the ionization chamber. Similarly, Figure 4.3 shows that the difference between the measured charge with and without the copper filter is negligibly small. This shows that the added copper filter does not affect the primary beam. For this reason, the copper filter is not necessary as long as the primary collimator is placed in the plateau region shown in Figures 4.2 and 4.3.

4.3 Radial distribution of the intensity of the collimated beam by the primary collimator

The average charge measured by the ionization chamber at various points across the vertical field, summarized in table 3.11, are plotted in Figure 4.4. Figure 4.5 shows the average charge measured by the ionization chamber at various points across the horizontal field, summarized in table 3.12. The error bar in each data point represents the standard deviation of the measured values at the given position of ionization chamber.

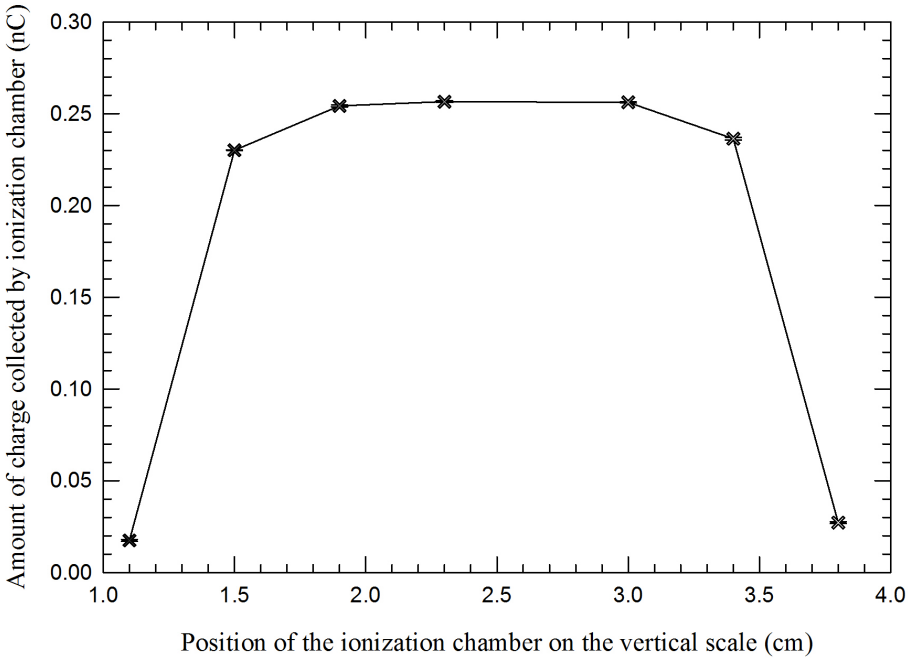

Figure 4.4: The measured charge by ionization chamber at various points across the vertical field of view.

We can see that the intensity of the beam outside the field of view drops by more than 90%. The cross-sectional size of the collimated beam as measured from the graph is about 1.9 cm × 4.3 cm which is greater than the dimensions of the collimator's aperture, 1.5 cm × 3.0 cm. The greater field of view of the collimated beam is due to

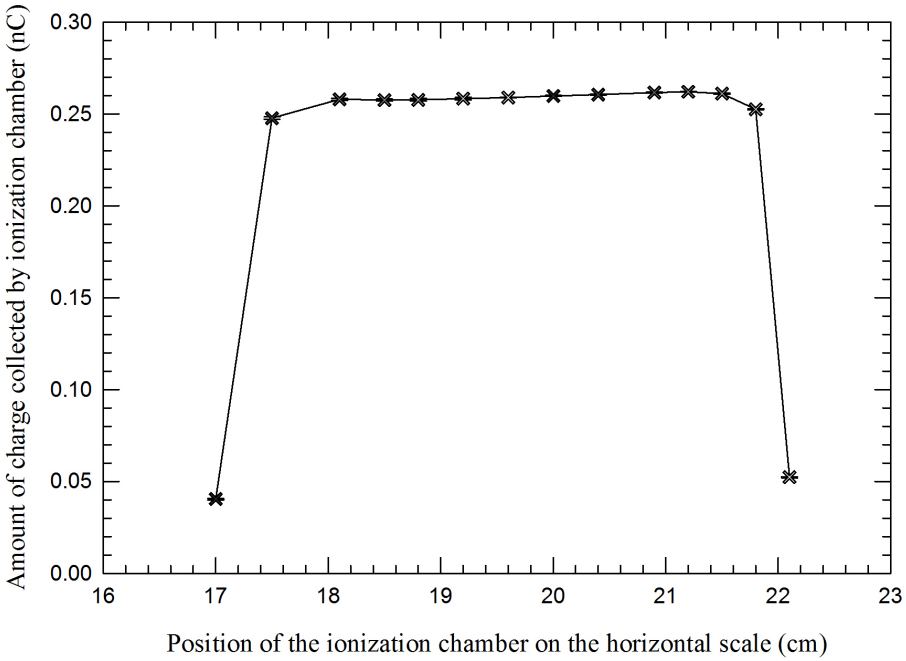

Figure 4.5: The measured charge by ionization chamber at various points across the horizontal field of view.

the diverging nature of the x-ray beam.

4.4 Radial distribution of the intensity of attenuated x-ray beam

Figure 4.6 shows a scattered plot of the average charge, listed in table 3.14, which was measured by an ionization chamber, placed at various points across the horizontal field of view. The horizontal axis shows the distance from the reference point to a position of the ionization chamber.

In Figure 4.7, the average charge measured at various points across the vertical field of view are plotted. The distance from the reference point to various positions of the ionization chamber The error bars represent the standard deviation of

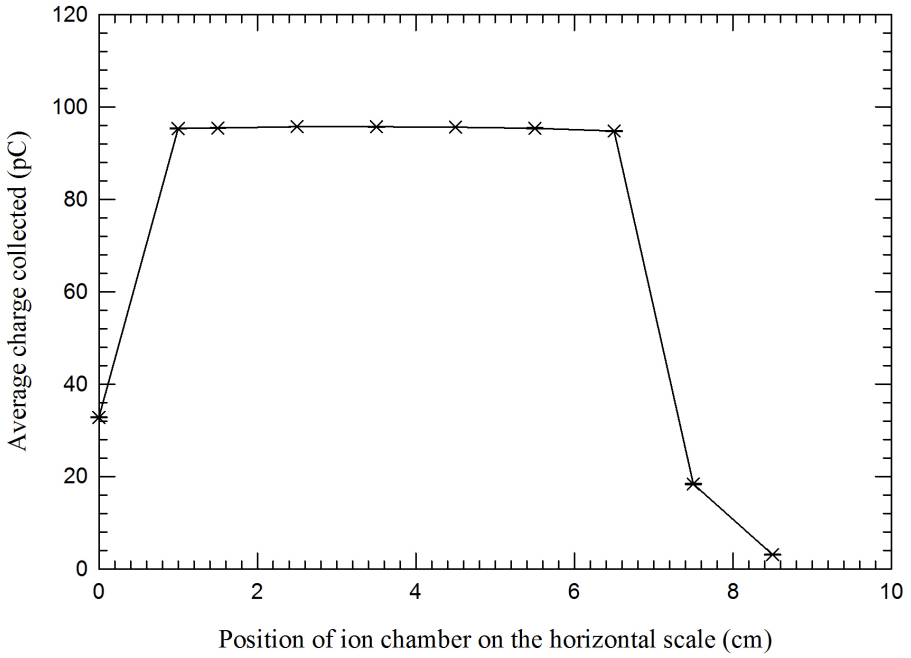

Figure 4.6: The average charge measured by an ionization chamber at various points along the horizontal field of view of the attenuated beam. The longitudinal distance from the source to the ionization chamber was 200 cm. The distance from the ionization chamber to the absorber was 46.3 cm and that to the primary collimator was 66.2 cm.

the values of the repeated measurements in a given position of the ionization chamber.

From the plots in Figure 4.6 and 4.7, we can see that the field size of the attenuated beam at a distance of 200 cm from the source or 46.2 cm from the absorber is about 3.0 cm $\times$ 5.5 cm. This suggests us the requirement of the secondary collimator so that the field size is reduced to the one which just covers the sensitive region of the PTW TN31014 ionization chamber.

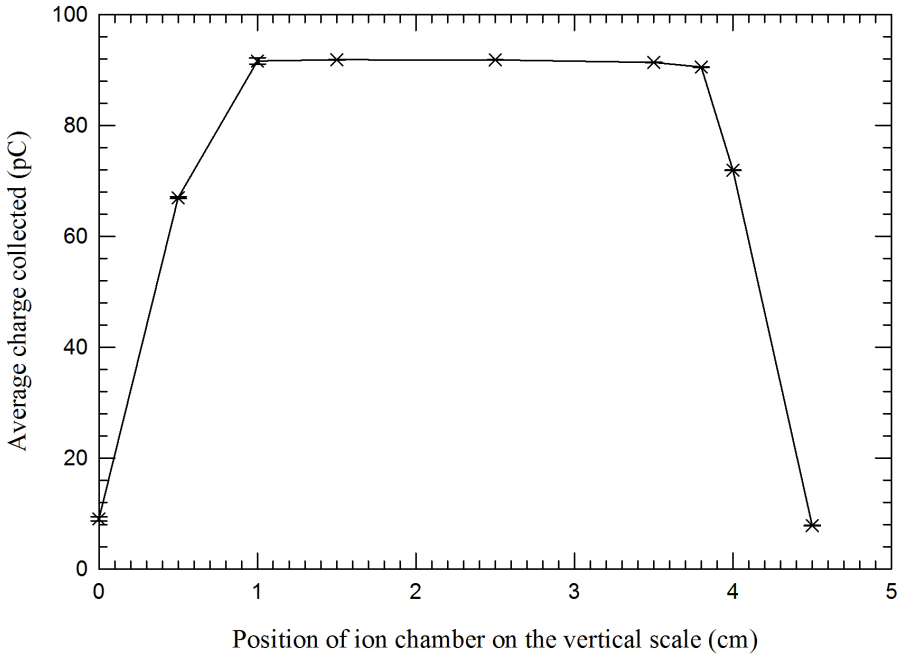

Figure 4.7: The average charge measured by an ionization chamber at various points along the vertical field of view of the attenuated beam. The longitudinal distance from the source to the ionization chamber was 200 cm. The distance from the ionization chamber to the absorber was 46.3 cm and that to the primary collimator was 66.2 cm.

4.5 Optimal position of the secondary collimator

Figure 4.8 shows a plot of the average charge (summarized in table 3.15) measured by the ionization chamber placed at a fixed distance of 200 cm from the source. The horizontal axis shows the distance from the source to the back surface of the secondary collimator. The primary collimator placed at a fixed position such that the distance from the source to the back surface of the primary collimator was 97.0 cm. The absorber was also placed at a fixed distance of 150 cm from the source. The error bar in each data point in the plot represents the standard deviation of the two measurements in a given position of the secondary collimator.

We can see from Figure 4.8 that the amount of charge collected by the ion-

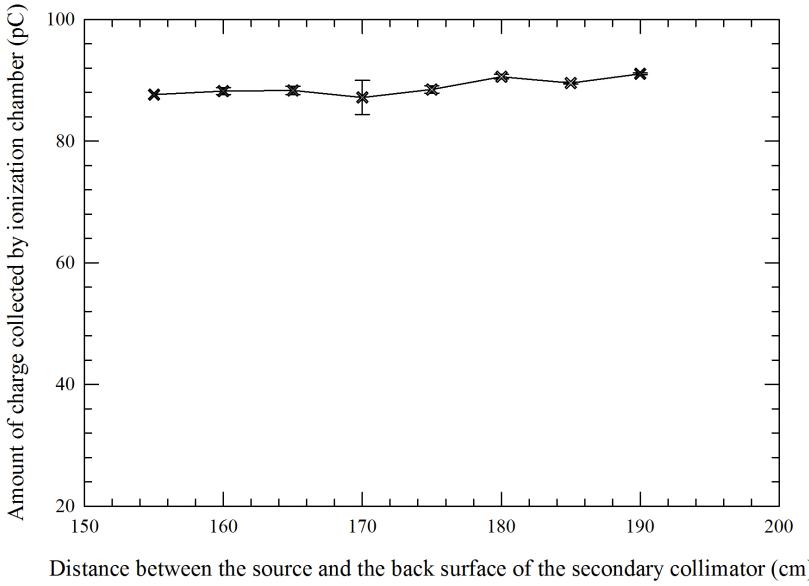

Figure 4.8: The amount of charge collected by an ionization chamber placed at 200 *cm* from the source with the secondary collimator placed at various positions, along the axis of the beam, in between the absorber and the ionization chamber.

ization chamber remains almost constant as the secondary collimator moves towards the ionization chamber and increases slightly when the collimator approaches the ionization chamber. The possible reason for a slight increment of the charge could be the secondaries produced from the inner surface of the collimator's aperture reach the ionization chamber. The graph indicates that the amount of secondary photons generated on the inner wall of the secondary collimator hole can be minimized by putting the secondary collimator at least 20 cm away from the ionization chamber.

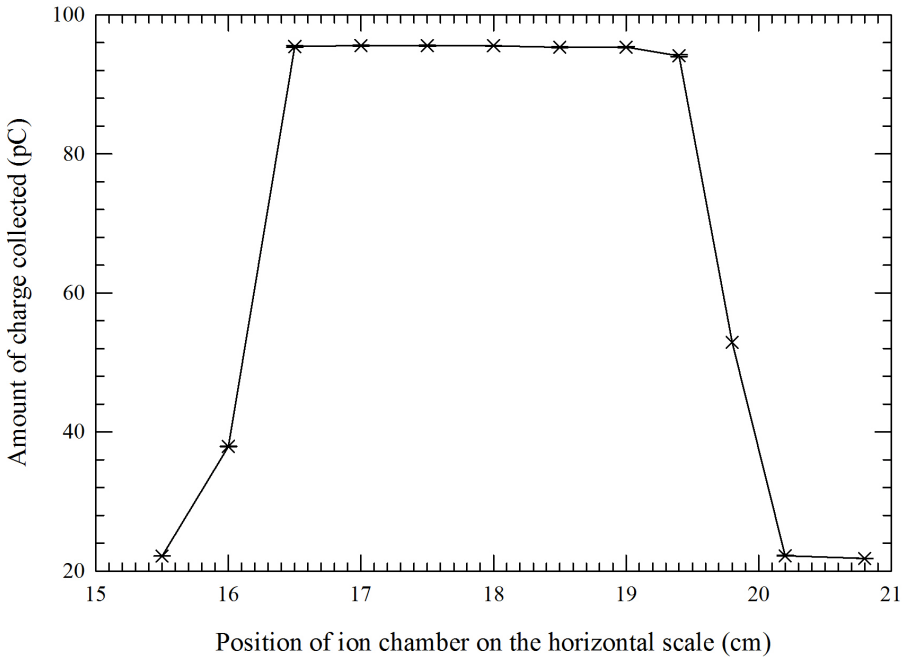

Figure 4.9: The average charge collected by an ionization chamber across the horizontal field of view of the beam beyond the secondary collimator.

4.6 Radial distribution of the intensity of the collimated beam beyond secondary collimator

The average charge collected by the ionization chamber across various positions of ionization chamber along the horizontal field of view is plotted in Figure 4.9 and that along the vertical field of view is plotted in Figure 4.10. The horizontal axis shows the distance from a reference point, taken arbitrarily outside the field of view of the beam, to the position of ionization chamber. The error bar in each point in the Figures 4.9 and 4.10 represents the standard deviation of two measurements in each position of the ionization chamber.

We can see from Figure 4.9 and 4.10 that the field of view of the beam at the position of the ionization chamber is about $1.5\,cm \times 3.0\,cm$ which was the desired

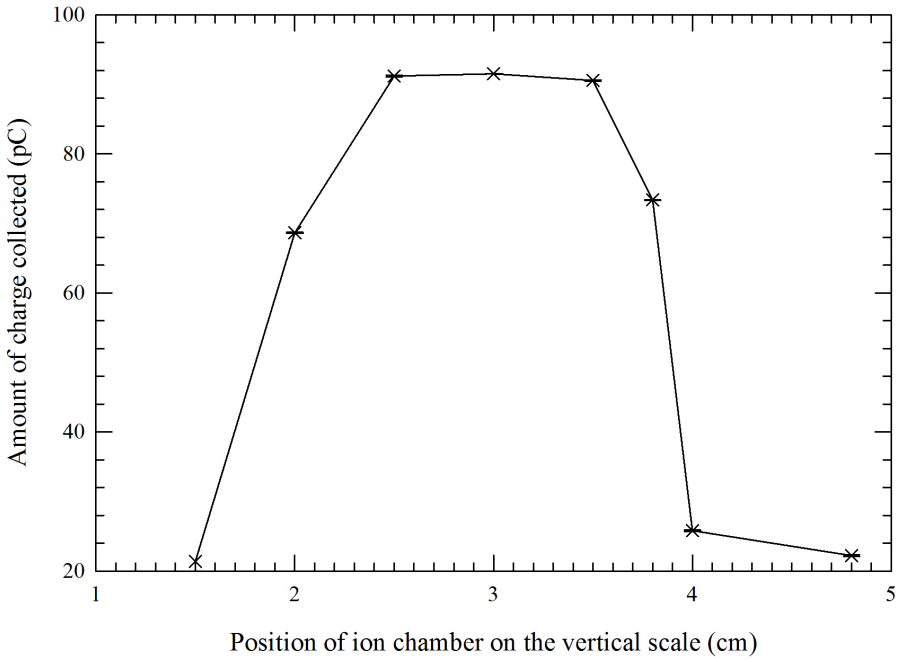

Figure 4.10: The average charge collected by an ionization chamber across the vertical field of view of the beam beyond the secondary collimator.

size as required by a narrow beam attenuation.

Chapter 5

CONCLUSION

The primary goal of this project was to design and test a set of collimators for the use in measuring attenuation data sets in therapeutic x-ray beams. The purpose of using collimators was to achieve a good geometry for a narrow beam attenuation so that the measured attenuation data sets can be used to estimate accurately the x-ray energy spectra.

While measuring attenuation data sets in therapeutic x-ray beams (4 MVp - 20 MVp), secondary x-rays are produced from three major interactions between the primary x-rays and the materials through which they penetrate. In a clinical linac, the source of x-rays (i.e. the electron target) is located inside the gantry and it produces diverging x-ray beams. The primary x-rays produced by the source travel through various components such as the flattening filter, the collimating jaws, any additional filters, etc. producing secondary x-rays that reach the detector. Secondary x-rays are also produced by the interaction between the primary x-rays and absorber. Secondary x-rays hence produced are either (i) the characteristic x-rays produced as a result of the photoelectric effect, (ii) the scattered x-rays as a result of the Compton effect, or (iii) the 511 keV photons as a result of the pair production. Since a detector cannot distinguish secondary x-rays from the primary x-rays, the secondary x-rays must be minimized by using some collimators.

Two collimators, a primary collimator and a secondary collimator, were

found essential to minimize secondary x-rays that reach the detector while measuring attenuation data sets in therapeutic x-ray beams.

The primary collimator was used in collimating x-ray beam before penetrating to the absorber. It was built using four different materials: lead, tin, copper and aluminum, in their respective order (descending Z). A thin copper filter was also used in the aperture of the primary collimator to absorb the characteristic x-rays produced by the inner surface of the aperture. The reason behind the use of multiple materials in the collimator was to absorb the secondary x-rays produced by the collimator itself.

In the primary collimator, the thickness of lead was chosen in such a way that the intensity of the x-rays that have minimum mass absorption coefficient on lead is reduced at least by a factor of 0.01. The factor of 0.01 was chosen arbitrarily. The thickness of tin in the primary collimator was chosen to minimize the secondary x-rays produced by lead by at least a factor of 0.01. Similarly, the thicknesses of copper and aluminum were chosen to absorb the secondary x-rays produced by tin and copper respectively.

The secondary collimator was built using only lead. Comparatively less amount of material was used in the secondary collimator as the primary collimator minimizes the secondaries that reach the absorber. The absorber further attenuates the secondaries before reaching the detector.

The dimensions of the aperture of two collimators were chosen in such a way that the collimated x-ray beam just covers the sensitive area of two PTW pin-point ionization chambers, each of type number 31014. These collimators can be used with any other detectors (ionization chambers) that have a sensitive area of approximately the same size as PTW TN 31014 ionization chambers. For detectors with smaller or larger radiation sensitive area, these collimators might not meet the requirements of a

narrow beam attenuation.

Various features of the primary and secondary collimators were studied considering a geometrical setup for the measurement of attenuation datasets as shown in Figure 5.1. The detector to measure the intensity of attenuated beam was placed at a fixed distance of 200 cm from the source and the absorber was placed at a fixed distance of 150 cm from the source.

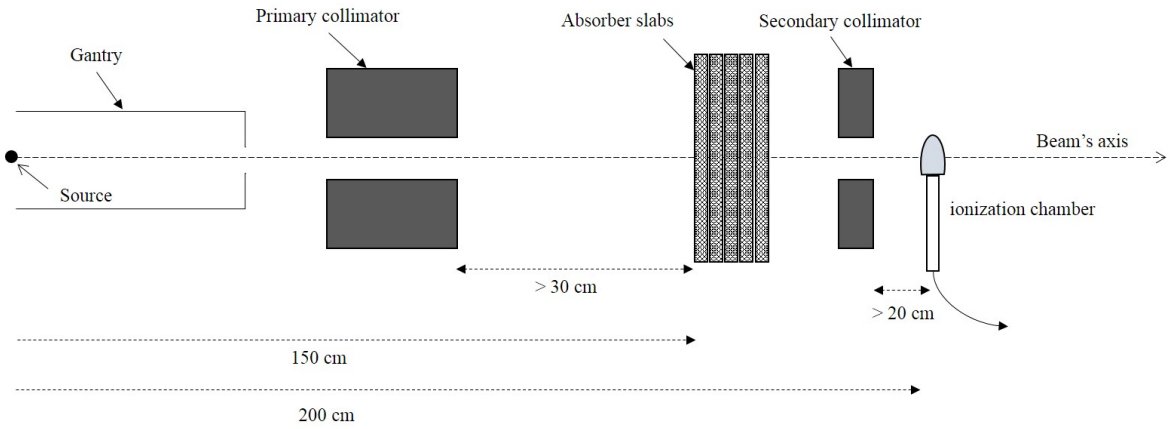

Figure 5.1: A schematic diagram showing a setup for use in measuring attenuation datasets in therapeutic x-ray beams.

It was found that the primary collimator should not be placed too close to the absorber so that the absorber receives minimum amount of secondaries produced by various components upstream the beam. Similarly the secondary collimator was found to minimize the secondaries when placed not too close to the detector. This agrees to an observation made by Dale et al. [17]: while measuring the half value layer of the primary x-rays on a material, the distance between the x-ray source and a detector must be made equal to twice the source to absorber distance. An increase in the number of secondaries that reach the detector, placed at a fixed distance from the source, can also be expected when the collimator is brought too close to the x-ray source. However, in this project none of the collimators could be placed too close to the x-ray source as the source was located deep inside the gantry.

In the experimental setup shown in Figure 5.1 where the distance from the source to the absorber is fixed at 150 cm, the primary collimator can be placed at least 30 cm away from the absorber. Similarly, by considering the space that the absorber materials occupy, the secondary collimator can be put at least 20 cm away from the ionization chamber. In this setup, the field of view of the collimated beam measured at the position of the ionization chamber was about 1.5 cm $\times$ 3.0 cm, the size of the collimator's aperture.

REFERENCES

[1] M. J. Berger, J. Hubbell, S. Seltzer, J. Chang, J. Coursey, R. Sukumar, D. Zucker, and K. Olsen, "Xcom: Photon cross sections database," *NIST Standard reference database*, vol. 8, no. 1, pp. 3587–3597, 1998.

[2] W. R. Hendee and E. R. Ritenour, *Medical imaging physics*. John Wiley & Sons, 2003.

[3] H. E. Johns, *Physics of radiology*. Charles River Media, 1983.

[4] K. Ng, C. Kwok, and F. Tang, "Monte carlo simulation of x-ray spectra in mammography," *Physics in medicine and biology*, vol. 45, no. 5, p. 1309, 2000.

[5] E. Y. Sidky, L. Yu, X. Pan, Y. Zou, and M. Vannier, "A robust method of x-ray source spectrum estimation from transmission measurements: Demonstrated on computer simulated, scatter-free transmission data," *Journal of applied physics*, vol. 97, no. 12, p. 124701, 2005.

[6] E. Ali and D. Rogers, "An improved physics-based approach for unfolding megavoltage bremsstrahlung spectra using transmission analysis," *Medical physics*, vol. 39, no. 3, pp. 1663–1675, 2012.

[7] R. G. Waggener, M. M. Blough, J. A. Terry, D. Chen, N. E. Lee, S. Zhang, and W. D. McDavid, "X-ray spectra estimation using attenuation measurements from 25 kvp to 18 mv," *Medical physics*, vol. 26, no. 7, pp. 1269–1278, 1999.

[8] L. Baird, "X-ray spectra vs attenuation data: A theoretical analysis," *Medical physics*, vol. 8, no. 3, pp. 319–323, 1981.

[9] P.-H. Huang, T.-S. Chen, and K. R. Kase, "Reconstruction of diagnostic x-ray spectra by numerical analysis of transmission data," *Medical physics*, vol. 13, no. 5, pp. 707–710, 1986.

[10] J. Boone, "X-ray spectral reconstruction from attenuation data using neural networks," *Medical physics*, vol. 17, no. 4, pp. 647–654, 1990.

[11] J. Twidell, "The determination of x-ray spectra using attenuation measurements and a computer program," *Physics in medicine and biology*, vol. 15, no. 3, p. 529, 1970.

[12] A. Iwasaki, H. Matsutani, M. Kubota, A. Fujimori, K. Suzaki, and Y. Abe, "A practical method for estimating high-energy x-ray spectra using the iterative perturbation principle proposed by waggener," *Radiation Physics and chemistry*, vol. 67, no. 2, pp. 81–91, 2003.

[13] F. H. Attix, *Introduction to radiological physics and radiation dosimetry.* John Wiley & Sons, 2008.

[14] F. M. Khan and J. P. Gibbons, *Khan's the physics of radiation therapy.* Lippincott Williams & Wilkins, 2014.

[15] M. Berger and S. Seltzer, "Xcom photon cross sections," *Version 3.1, NISTIR*, 1999.

[16] A. Jacobson, B. M. Birkhead, and R. M. Scott, "Correlation of physical characteristics of 4 mv x-ray beams with skin reactions of patients undergoing radiation therapy 1," *Radiology*, vol. 112, no. 1, pp. 203–207, 1974.

[17] E. D. Trout, J. P. Kelley, and A. Lucas, "Determination of half-value layer." *The American journal of roentgenology, radium therapy, and nuclear medicine*, vol. 84, pp. 729–740, 1960.

VITA

Rajesh Panthi

Candidate for the Degree of

Master of Science

Thesis: DESIGN AND TESTING OF COLLIMATORS FOR USE IN MEASURING X-RAY ATTENUATION

Major Field: Medical Physics

Biographical:

Education:

Completed the requirements for the Master of Science in Medical Physics at Oklahoma State University, Stillwater, Oklahoma in December, 2017.

Completed the requirements for the Master of Science in Physics at Tribhuvan University, Kathmandu, Nepal in July 2009.

Completed the requirements for the Bachelor of Science in Physics, Mathematics, and Statistics at Tri-Chandra Campus, Kathmandu, Nepal in November 2004.

Experience:

Teaching and Research Assistant Oklahoma State University Stillwater, OK	08/2011-Present
Lecturer of Physics St. Xavier's College Kathmandu, Nepal	08/2009-06/2011

Professional Memberships:

American Association of Physicists in Medicine (AAPM)
American Physical Society (APS)